Numerical Analysis of Reinstallation of Spudcans near Footprints Formed during Prior Installations

M. J. Jun[1], Y. H. Kim[2], M. S. Hossain[3], M. J. Cassidy[4], Y. Hu[5] and S. G. Park[6]

[1]Principal Researcher (PhD), Daewoo Shipbuilding & Marine Engineering Co. Ltd. (DSME), 96, Baegot 2-ro, Siheung-si, Gyeonggi-do, Republic of Korea Tel: +82 (0)2 2129 3790, Email: mjjun@dsme.co.kr

[2]Corresponding Author, Research Fellow (PhD), Centre for Offshore Foundation Systems (COFS), Oceans Graduate School, The University of Western Australia, 35 Stirling Highway, Crawley, WA 6009, Australia, Tel: +61 (0)8 6488 4316, Email: youngho.kim@uwa.edu.au

[3]Associate Professor (BEng, MEng, PhD, MIEAust), Centre for Offshore Foundation Systems (COFS), Oceans Graduate School, The University of Western Australia, 35 Stirling Highway, Crawley, WA 6009, Australia, Tel: +61 (0)8 6488 7358, Email: muhammad.hossain@uwa.edu.au

[4]Professor (FTSE, FIEAust, GAICD, DPhil), Dean and Professor of Civil Engineering, Melbourne School of Engineering, Doug McDonell Building, The University of Melbourne, Victoria 3010, Australia, Tel: +61 3 8344 6619, Email: mark.cassidy@unimelb.edu.au

[5]Professor (PhD, MIEAust), School of Civil, Environmental and Mining Engineering, The University of Western Australia, 35 Stirling Highway, Crawley, WA 6009, Australia, Tel: +61 (0)8 6488 8182, Email: yuxia.hu@uwa.edu.au

[6] Principal Researcher (MS), Daewoo Shipbuilding & Marine Engineering Co. Ltd. (DSME), 96, Baegot 2-ro, Siheung-si, Gyeonggi-do, Republic of Korea Tel: +82 (0)2 2129 3511, Email: sgpark8@dsme.co.kr

- Number of Words: 4653 (text only)
- Number of Tables: 02
- Number of Figs.: 18

Numerical Analysis of Reinstallation of Spudcans near Footprints Formed during Prior Installations

ABSTRACT

This paper reports the effect of the remoulded soil strength of a footprint on the reinstallation of jack-up rigs near the footprint. The footprint creation is from an earlier spudcan penetration and extraction process in which the soil is remoulded. Dissipation of pore pressures between the footprint creation and jack-up reinstallation causes further consolidation of the soil around the footprint. Large-deformation finite-element (LDFE) analyses were performed using the Coupled Eulerian-Lagrangian (CEL) approach. A recently developed novel spudcan shape with a flat base and four holes is studied to mitigate spudcan-footprint interactions during spudcan reinstallation. The installation of a whole three-legged jack-up rig is modelled considering a simplified global jack-up unit. The LDFE results were validated against existing centrifuge test data prior to undertaking a detailed parametric study, assessing the effects of consolidation occurred after footprint creation, the offset distance of spudcan installation from the footprint centre, and spudcan shape. Compared to a footprint of the same shape, but virgin intact soil strength, the footprint with remoulded soil strength enhances the maximum horizontal force, maximum moment, maximum lateral displacement, and rotation, by 12~20%. The critical offset distance is found to be one spudcan diameter with the spudcan centre being at the crest of the footprint. The novel spudcan shape is shown to be effective at easing spudcan-footprint interactions, reducing horizontal force, moment, lateral displacement and rotation by about 50%; and total stress on the jack-up leg by 41%.

Keywords: jack-up, spudcan-footprint interaction, spudcan, remoulded soil strength, numerical modelling

1. INTRODUCTION

Modern jack-ups typically consist of a buoyant triangular platform supported by three independent truss legs, each attached to a large-diameter spudcan. After completing the planned operation at a site, the legs are retracted from the seabed, which leave depressions - referred to as a crater or 'footprint'. Jack-ups often return to the previous operation site for further drilling where the footprints from previous explorations are present. Where one of the jack-up legs is located near an existing footprint slope, there is a tendency for the spudcan to slide towards the centre of the footprint, inducing excessive lateral displacements and bending moments or rotations of the rig. These detrimental foundation behaviours can result in an inability to install the jack-up at the required position, and even worse the occurrence of leg splay and structural damage to the whole jack-up system. The frequency of offshore incidents during installation near footprints has increased by a factor of four from the period 1979~88 to the period of 1996~2005 [1]. MSL [2] also reported the spudcan-footprint interaction as the second most common reason for jack-up foundation failures.

To investigate this issue, the characteristics of spudcan-footprint interactions have been investigated by a number of researchers, mostly through physical modelling. Leung et al. [3] and Gan et al. [4] presented the effect of time on the recovery of remoulded soil strength by using centrifuge tests. Gaudin et al. [5] focused on large lateral sliding towards the footprint centre considering remoulded soil strength profiles. Cassidy et al. [6] addressed the effects of leg stiffness, offset distance and remoulded soil zone on spudcan-footprint interactions. Kong et al. [7,8] studied this issue considering a footprint with intact soil strength (i.e. not affected by remoulding and reconsolidation), and the typical failure mode was addressed through centrifuge observation and subsequent particle image velocimetry analyses. Hossain and Stainforth [9] and Hossain et al. [10] have assessed the performance of perforation drilling

and spudcan shapes on easing spudcan-footprint interactions considering a footprint with intact soil strength.

Recently the spudcan-footprint interaction problem has been addressed through numerical modelling. Zhang et al. [11] and Jun et al. [12,13] investigated this issue through large deformation finite element (LDFE) simulations, by considering the artificial footprint geometry with intact soil strength. Hartono et al. [14] and Tho et al. [15] also carried out LDFE analysis by generating the footprint through the spudcan extraction process. However, due to the limitation of the used constitutive models, the effect of time or generation and dissipation of excess pore pressure has not been captured. Furthermore, the proper suction at the base of the originally extracting spudcan has not been modelled, leading to "immediate breakaway" condition [16,17]. It should be noted that, in clay, suction at the base of the extracting spudcan constitutes the reverse end bearing soil flow up to a significant extraction distance, and is the major contributor to the extraction resistance [18-20].

Unlike spudcan penetration into a flat seabed, the excessive horizontal force and moment induced by the spudcan-footprint interaction may cause a global lateral or rotational movement of the whole jack-up rig. However, in the reported physical and numerical modelling, a single leg connected with a flat plate or generic spudcan, and fixed head condition at the top of the leg [3,4,6-8,11-13] or free head condition that allows sliding of the leg [5,9,10] has been considered. Recently, Jun et al. [21] developed a simplified global jack-up modelling framework for examining the three-dimensional global response of a jack-up rig induced by spudcan-footprint interactions.

In this paper, a series of three-dimensional LDFE analyses were carried out to investigate the effect of spudcan-footprint interactions. Due to the limitations noted previously, the footprint was not created in the real field way of penetrating and extracting a spudcan. Instead, the measured soil strength profiles and footprint geometries from a centrifuge test [4], were

99 directly mapped in the LDFE simulations. It is the first attempt to idealise the formation of a
100 footprint shape and remoulded soil strength which depends on the soil strength, spudcan
101 penetration depth (or preload), jack-up operation time and elapsed time between the initial
102 extraction and re-installation. In addition, the global jack-up modelling framework was also
103 incorporated. The novelty of this paper lies in coupled considerations of (i) a real footprint
104 shape with remoulded soil strength contour around, instead of idealised intact soil strength,
105 and (ii) global jack-up response, rather than a single leg, which are proved later to be crucial
106 for capturing realistic spudcan-footprint interactions. The performance of a novel spudcan
107 shape in easing spudcan-footprint interactions was tested.
108

109 **2. NUMERICAL ANALYSIS**

110 3D LDFE analyses were carried out using the coupled Eulerian-Lagrangian (CEL) approach
111 in the commercial Finite Element (FE) package ABAQUS/Explicit [22]. Extensive
112 background information about spudcan installation modelling can be found in Jun et al.
113 [12,13], Hu et al. [23] and Zheng et al. [24], and but is not repeated here.

114 An extensive parametric investigation was undertaken varying the relevant range of
115 parameters, such as the (a) remoulded soil zone and strength underneath a footprint surface; (b)
116 elapsed time (ET: time between the formation of a footprint or extraction of a spudcan and re-
117 installation of a spudcan) i.e. effect of re-consolidation through dissipation of the induced
118 excess pore pressure; (c) offset distance (β: distance between the footprint centre and
119 reinstalling spudcan centre); and (d) spudcan shapes. Finally, the effect of a prior spudcan
120 installation on spudcan-footprint interactions was quantified for each parameter by comparing
121 with the results for an artificial footprint with intact soil strength.

2.1 Modelling of spudcan-footprint interactions

Considering the symmetry of the problem, half of the spudcan and soil were modelled. The lateral extension of the soil domain was 4.5D from the centre of the footprint (D is the spudcan diameter) on the spudcan penetration side and 2.5D on the opposite side, and the depth of the soil domain was ~5.5D to avoid boundary effects during the installation process (as obtained from preliminary convergence studies and considered by researchers including Jun et al. [12] and Zheng et al. [24]). The footprint geometry and corresponding remoulded soil strength were directly imported from centrifuge data [4]. The typical soil element size along the trajectory of the spudcan (i.e., in the fine mesh zone) was selected as 0.025D based on the mesh convergence study reported by Jun et al. [12]. A typical mesh is shown in Fig. 1. The spudcan was simplified as a rigid body and connected to a simplified jack-up rig model. The penetration velocity of the spudcan in the numerical analysis (v_{LDFE}) was taken as 0.1 m/s. In the analyses using the CEL approach, it was necessary to avoid inertial effect. Even in a rate independent (and non-softening) ideal soil, the penetration resistance was found to increase with increasing v_{LDFE} due to the inertial effect. A series of sensitivity analyses has led to select the value of 0.1 m/s. This is consistent with the conclusions drawn by Qiu & Henke [25], Hu et al. [26], Tho et al. [27] and Zheng et al. [28], who adopted a penetration velocity of 0.5, 0.2, 0.1672 and 0.1 m/s, respectively.

The reinstallation of spudcans in clay is completed under undrained conditions. In addition, clay exhibits strain-rate dependency due to viscous rate effect and also softens as it is sheared and remoulded. Thus, following the work of Einav and Randolph [29], the soil was modelled as an elasto-perfectly plastic material that obeys a Tresca yield criterion with extensions to capture the strain rate and strain-softening effects as

$$s_u = \left[1 + \mu \log\left(\frac{\mathrm{Max}\,(|\dot{\gamma}|,\dot{\gamma}_{ref})}{\dot{\gamma}_{ref}}\right)\right]\left[\delta_{rem} + (1-\delta_{rem})e^{-3\xi/\xi_{95}}\right]s_{u,ref} \quad (1)$$

The parameter definitions are given in the notation list. The maximum shear strain rate, $\dot{\gamma}$, was deduced by dividing the computed maximum shear strain ($\Delta\varepsilon_1 - \Delta\varepsilon_3$) by the notional time increment, Δt_N. To reflect the effect of strain rate related to the field, the notional time period at each increment (Δt) is amended by the ratio of spudcan penetration velocity or strain rate in the LDFE analysis (v_{LDFE}/D_{LDFE}) to the typical one in the field (v_{field}/D_{field}) according to

$$\Delta t_N = \frac{\delta_{LDFE}/D_{LDFE}}{v_{field}/D_{field}} = \frac{v_{LDFE}\Delta t/D_{LDFE}}{v_{field}/D_{field}} = \left(\frac{v_{LDFE}/D_{LDFE}}{v_{field}/D_{field}}\right)\Delta t \quad (2)$$

In this study, an equal spudcan diameter was considered for LDFE analysis and field i.e. $D_{LDFE} = D_{field}$. The reference strain rate, $\dot{\gamma}_{ref}$, was considered as 1.5%/h, and as such the normalised penetration rate ($v_{field}/D_{field}\dot{\gamma}_{ref}$) of 8.88 lied within the range of practical interest (4 ~ 20) [24, 30]. It should be noted that typical values of spudcan penetration rate in the field may be estimated to lie between 0.4 and 4 m/h, and reference shear strain rate in triaxial test ranges from 1%/h to 4%/h. Further details can be found in Hossain and Randolph [30], Zheng et al. [24] and Kim and Hossain [31].

The soil-spudcan interface was modelled as frictional contact, using a general contact algorithm with Coulomb friction law. Two different contact properties were applied for the side and bottom of spudcan, respectively. For the side friction of skirt and holes, the Coulomb friction coefficient was set to a high value of $\mu_C = 50$, in order to allow the value of τ_{max} (= αs_u; where α is the frictional ratio taken as the inverse soil sensitivity, $1/S_t$) to govern failure [32, 33]. For the friction between the bottom profile of spudcan and footprint slope, μ_C was taken as 0.1, without τ_{max} specified on the interface [34-36].

A simplified global jack-up rig modelling technique was adopted to consider the behaviour of a whole jack-up rig including three legs and corresponding spudcans. The technique was developed and detailed by Jun et al. [21], and as such, was not repeated here. Jun et al. [21]

considered both simultaneous and leg-by-leg preloading and found insignificant effect of the preloading process. In this study, leg-by-leg preloading process was adopted. To reduce the computational time, the spudcans on the flat ground were replaced by initial foundation springs / stiffness (e.g., K_V, K_H, K_M; from ISO, 2012 and Jun et al., 2019). Note, ISO guidance [37] recommends using a secant reduced rotational stiffness to ensure compliance with the yield interaction surface. However, a secant stiffness model is not applicable for penetrating foundations. In this penetration analysis, the rotational reaction induced by the spudcan-footprint interaction is relatively very small, compared to the extreme condition from structural integrity tests. Furthermore, the effect of the reduced rotational stiffness will be compensated by the buoyance spring. As such, for the considered problem with spudcan continuous penetration with initial foundation springs / stiffness (K_V, K_H and K_M) were adopted. Actual global modelling is shown in Fig. 2. Note that other environmental loads induced by winds, waves and currents were ignored, as it is common that a preloading is planned for relatively calm weather conditions [38].

3. VALIDATION ANALYSIS AGAINST CENTRIFUGE TEST

The LDFE modelling techniques were validated against previously published centrifuge test data (Group I, Table 1). Gan et al. [4] carried out a series of centrifuge tests at 200g to evaluate the effect of time on spudcan-footprint interactions in kaolin clay. The soil strength profiles before spudcan penetration (i.e., intact soil strength: $s_{u,ref}$) and after extraction (i.e., remoulded soil strength: $s_{u,remoulded}$) were deduced from ball penetrometer tests and plotted using remoulded strength ratio, $R_{su} = s_{u,remoulded}/s_{u,ref}$ (see Fig. 3). The slope across the footprint was also measured by a laser scanning device. For the validation exercise, the over-consolidated clay case ($s_{u,ref} = 5 + 1.8z$ kPa) with the operating time (OP) = 0 year and elapsed time (ET) = 1.0 year was selected. The soil strength contour, remoulded zone and surface

slope of the footprint were extracted from the test data and then mapped in the LDFE modelling, as shown in Figs. 4a and 4c. The simplified soil strength contour plotted in Figs. 4b and 4c has fewer mapping zones and is used for the comparison of results. The soil strength parameters in Fig. 4 and the soil strain parameters of $\mu = 0.1$, $\delta_{rem} = 1/S_t = 1/3$, $\xi_{95} = 15$, and $\dot{\gamma}_{ref} = 1.5\%\ h^{-1}$ were used in LDFE analyses. Note, the soil strain parameters depend on the soil condition, i.e. remoulded or disturbed soil from prior installation and plastic shear strain. However, the soil strain parameters from the original intact strength were adopted here due to the lack of the test data for this remoulded soil. The spudcan was penetrated at an offset of $\beta = 0.5D$ from the footprint centre with a constant penetration rate of 0.1 m/s. The same spudcan (D = 14.54 m; see inset in Fig. 3) and boundary condition (fixed head condition) were considered following Gan et al. [4]. An analysis was also performed considering the global jack-up rig and simplified soil strength contour.

The results of the analyses are plotted in Fig. 5 in terms of horizontal force (H), vertical force (V) and bending moment (M) distributions as a function of the normalised spudcan base penetration depth, d/D. The computed horizontal, vertical and moment responses from the current LDFE technique are in reasonable agreement with the measured data from Gan et al. [4]. This validation exercise confirmed the capability and accuracy of the CEL approach in assessing responses during the penetration of a spudcan adjacent to an existing footprint.

The detailed mapping (see Fig. 4a) with more soil strength layers made the simulation computationally expensive (e.g., 4.5 weeks for a spudcan penetration up to 0.8D, with a high performance PC with 8 CPU cores and 8.0 GB memory). The numerical stability of the CEL approach was ensured by ABAQUS/Explicit [22] introducing a critical time increment $\Delta t_{critical}$. The value of $\Delta t_{critical}$ can be approximately estimated by L_{min}/c_d, where L_{min} is the minimum element dimension in the Eulerian meshes and c_d is the dilatational wave speed of the material. A slight decrease in $\Delta t_{critical}$ increases the computational time significantly [39]. Since the

detailed soil strength contour has a complex curve shape (see Figs. 4a), a small value of L_{min} (or $\Delta t_{critical}$) and a massive number of soil elements (to ensure accuracy) were the result, and hence a computational time was very costly. The computational time was reduced by up to 56% without reducing $\Delta t_{critical}$ when the soil strength contour was simplified, as shown in Fig. 4b. The effect of the global modelling was quantified by comparing with the results for the fixed head condition (simplified strength contour). The maximum horizontal force (H_{max}) and moment (M_{max}) for the global modelling are 0.87 MN and 15.1 MN-m, which are approximately 10 and 13% lower, respectively, than those of the fixed head condition (see Figs. 5b and 5c). These reductions arise mainly from the lateral sliding towards the footprint centre (see Fig. 5d) and the rotation of the spudcan (see Fig. 5e). Based on this exercise, simplified soil strength contour and global modelling technique were adopted for subsequent analyses.

4. RESULTS AND DISCUSSION: PARAMETRIC STUDY

To examine the effect of various factors on jack-up rig spudcan-footprint interactions, an extensive parametric study was carried out varying the (a) remoulded soil zone (b) elapsed time between footprint creation and reinstallation (ET = 1 year and 100 years); (c) offset distance (β = 0.25D ~ 1.25D); and (d) spudcan shape (generic spudcan and novel spudcan; D = 15 m). The intact undrained shear strength of soil ($s_{u,ref}$ = 5 + 1.8z kPa) and the outer diameter of spudcans (D = 15 m) were kept constant. The results from this parametric study, as assembled in Table 1, are discussed below.

4.1 Effect of remoulded soil zone from initial penetration

The effect of the remoulded soil zone from the initial penetration-extraction of the spudcan was investigated by comparing the results considering a footprint with the remoulded zone or

241 simplified strength contour (see inset in Fig. 6a) and a footprint with undisturbed or intact soil
242 strength (see inset in Fig. 6b; Group II, Table 1). The shape of the generic spudcan (see inset
243 in Fig. 6a) was chosen to be similar to the spudcans of the 'Marathon LeTourneau Design,
244 Class 82-SDC' jack-up rig, as illustrated by Menzies & Roper [40]. The offset distance was
245 fixed at $\beta = 0.5D$. The remoulded soil strength profiles adopted were identical to those from
246 Section 3 (ET = 1 year).
247 Fig. 6 shows the comparison responses in terms of the vertical force (V), horizontal force (H),
248 moment (M), eccentricity (e), lateral displacement (δ_H) and rotation (θ) distributions along the
249 normalised penetration depth (d/D). As expected, the penetration resistance (i.e. vertical force,
250 V) for the footprint with intact soil strength is higher than that with remoulded soil strength
251 due to weakening of the remoulded footprint ($R_{su} < 1.0$). After the spudcan passes the
252 remoulded zone ($R_{su} = 1.0$), the gap between these two profiles tends to diminish. This is not
253 too obvious for the vertical force profile (Fig. 6a) but more evident for the horizontal force
254 and moment profiles (Figs. 6b and 6c).
255 Interestingly, the maximum horizontal force (H_{max}) for the footprint with remoulded soil
256 strength is around 1.02 MN, which is about 14.6 % higher than that for the footprint with
257 intact soil strength ($H_{max} = 0.89$ MN), and that occurs at a much deeper penetration depth of
258 $d_{Hmax}/D = 0.338$ compared to $d_{Hmax}/D = 0.065$ for the footprint with intact soil strength. To
259 explain, Fig. 7 shows an example of mobilised imbalance force (F_{imb}) on the right hand side
260 of the spudcan induced by the difference R_{su} (δR_{su}). F_{imb} could be proportional the values of
261 '+ve' δR_{su} as well as the area of '+ve' δR_{su} ($A_{\delta Rsu}$) (see Fig. 7a). This imbalance force
262 induced the additional horizontal force (see inset in Fig. 7b). The corresponding failure
263 mechanisms, soil strength contour line and schematic diagram of imbalance force at different
264 stages of penetration are illustrated in Fig. 8. For the footprint with intact soil strength, the
265 imbalanced horizontal force is mostly induced by the difference in bottom contact area

between the side of the spudcan closest to the centre of the footprint and the one furthest (left and right side of the spudcan, as depictied in the diagrams of Fig. 7). For instance, at d/D = 0.065 where H_{max} occurs, the right hand side of the spudcan with the intact soil is fully contacted around the footprint surface and the left hand side is partly touched (see Fig. 8a). With further penetration, d/D = 0.338, the horizontal force is reduced with the increase in the contact area of the left hand side of the spudcan base (see Fig. 8b). For the footprint with remoulded soil, at the initial penetration stage, the difference in the contact area between the left and right hand side of the spudcan base is also large around the footprint surface (see Fig. 8a). However, the induced horizontal force is relatively small due to the very low surface soil strength (R_{su} = 0.2). With further penetration, although both sides of the spudcan are fully contacted (see Fig. 8b), the horizontal force gradually rises due to the difference in the remoulded soil strength between the left and right hand side of the spudcan base (see Fig. 8b).

The moment (M) distributions show a slightly different trend, compared to the horizontal force (H). With the reference point at the centre of the spudcan (see RP in Fig. 6), the bending moment (M) on the spudcan is induced only by the resultant vertical force and eccentricity thereof, as the resultant horizontal force H nearly passes through the RP [7,11,12]. As shown in Figs. 6c and 6d, a slightly larger maximum moment (M_{max}) for the footprint with intact soil is due to this larger eccentricity of the resultant vertical force (see Fig. 6d). The lateral displacement and rotation at the RP are shown in Figs. 6e and 6f. The overall tendency of these parameters are consistent with the one for horizontal force.

In the field, spudcan-footprint interactions generally result in the buckling of the leg at just below the hull because of the additional bending moment M_a (= H × leg length (L_{leg}) + V × leg eccentricity (e_{leg}); see Fig. 9a). The corresponding reference point is RP1, as shown in Fig. 9a. The horizontal and vertical forces are not affected by this change of the RP. The profile of the total moment about RP1, $M_t = M + M_a$, was extracted from the global modelling by using

291 'sectional force' of each equivalent leg. The profiles moment about RP and RP1 are plotted in
292 Fig. 9b, and the values of the maximum moment, M_{max} and $M_{t,max}$, are tabulated in Table 1.
293 The values of $M_{t,max}$ are 698% (for the footprint with intact soil strength) and 820% (for the
294 footprint with remoulded soil strength) higher compared to M_{max}. In addition, and
295 interestingly, the absolute value of $M_{t,max}$ for the footprint with remoulded soil strength is 12.4%
296 smaller compared to that for the footprint with intact soil strength, which is now consistent
297 with enhancement of H_{max}. This can have a significant impact on the performance of the leg
298 structure members, which will be discussed later (Section 4.4).

299 **4.2 Effect of elapsed time**

300 To examine the effect of elapsed time ET, additional analyses were performed for ET = 100
301 years (operating time, OP = 0; Group III, Table 1). The corresponding recovered soil strength
302 contour from Gan et al. [4] is plotted in Fig. 10. Compared to the strength contour for ET = 1
303 year (Figs. 3 and 4), the size of the remoulded zone is shallower due to recovery of strength
304 through reconsolidation or dissipation of the induced excess pore pressure. However, there is
305 a strengthened zone at ~0.4D below the footprint tow, with the soil strength higher than that
306 of the intact soil strength (R_{su} = 1.2). Gan et al. [4] attributed this strengthening to the
307 squeezed soil volume and increase in effective shear strength during operation and the long
308 elapsed time, which fully dissipated the excess pore pressure under the spudcan.
309 Fig. 11 shows the comparison responses between ET = 1 year and 100 years. The
310 corresponding schematic diagram of imbalance force, failure mechanism and contour line of
311 soil strength for ET = 100 years are displayed in Fig. 12. The vertical force (V) profile for ET
312 = 100 years lies above the one for ET = 1 year due to higher recovered strength. The
313 maximum horizontal force (H_{max}) and moment (M_{max}) about RP1 for ET = 100 year are
314 smaller although the soil strength beneath the spudcan is larger. This is attributed to the size

of the remoulded zone beneath the spudcan and the difference in soil strength between the left and right hand side of the spudcan (see Figs. 8b and 12). Below the initial penetration depth (d_e) or the penetration depth during creating the footprint, the long-term case shows a negative horizontal force and moment profile (see Figs. 11b and 11c), due to the presence of the strengthened zone (R_{su} = 1.2; Fig. 10). The lateral displacement and rotation distributions also agree well with this opposite trend (Figs. 11d and 11e).

In summary, with increasing elapsed time (and hence recovering soil strength), the size of the remoulded zone, created by initial penetration and extraction, reduced gradually, leading to a reduction in the imbalanced soil strength between the left and right hand side of the spudcan, and hence in maximum horizontal force and moment. A consistent tendency was reported by Gan et al. [4] analysing centrifuge model test data.

4.3 Effect of offset distance

In order to show the effect of offset distance, spudcan penetration response profiles are plotted in Fig. 13 for a range of β from 0.25D to 1.25D, but with identical elapsed time of ET = 1 year and operating time OP of 0 year (Group IV; Table 1). The magnitude of the vertical force (V) increases with the offset distance β (Fig. 13a) as a result of reducing the influence from the remoulded zone. The horizontal force (H) profiles for each offset distance β are presented in Fig. 13b. Very interestingly, however, the values of H_{max} increases with increasing β up to β = 1.0D (H_{max} = 1.31 MN) and then drops to 0.99 MN for β = 1.25D. This trend is true for maximum moment M_{max} (about RP1), maximum lateral displacement δ_H and maximum rotation θ (see Figs. 13b to 13e). This can be explained by the imbalanced force between the right and left hand side of the spudcan base due to the distribution of the remoulded soil strength. Fig. 14 shows a schematic diagram of the imbalance force, failure mechanism and contour lines of soil strength ratios at a depth of H_{max} for each offset distance

β. It can be seen that the difference in the remoulded soil strength between left and right hand sides of the spudcan base increases as the spudcan reinstallation moves from near the footprint centre to the footprint crest or β increases from 0.25D to 1.0D (Fig. 14a to 14c). However, once the spudcan moves away from the footprint crest i.e., β = 1.25D (Fig. 14d), the presence of intact soil strength on both sides of the spudcan base reduced the imbalance force.

Fig. 15 plots H_{max} normalised by the largest value of H_{max} among the various offset distances ($H_{max,\beta max}$) as a function of normalised offset distance (β/D). The existing results from centrifuge tests reported by Cassidy et al. [6], Stewart and Finnie [41], Gan [42], Hartono [43] and from LDFE analyses by Zhang et al. [11] are also included for comparison. The information in regards to spudcan diameter and shape, initial penetration depth during creating footprint, d_e, and intact soil strength ($s_{u,ref}$) profile for these existing investigations are summarised in Table 2. Regardless of the variation in intact strength, initial penetration depth, and spudcan shape and diameter; the values of $H_{max}/H_{max,\beta max}$ show reasonably a unique trend, with the critical offset distance (β) lies between 0.5D ~ 1.0D from the centre of the footprint.

4.4 Effect of novel spudcan shape

In this study, the generic spudcan shape was used in all the analyses already presented. This section assesses the performance of a novel spudcan shape on easing spudcan-footprint interactions and the consequent influence of this shape on the structural integrity of the jack-up leg. Currently, there are several mitigation methods reported, including (a) infilling the crater [44-46]; (b) stomping [14,44,43,47]; (c) reaming [14,43,47]; (d) perforation drilling [9]; and (e) simultaneous water jetting and spudcan preloading [48]. However, all these methods require additional work on the seabed prior to spudcan re-installation, leading to additional cost and time to be applied in the field. Recently, Hossain et al. [10] and Jun et al. [12]

studied the effect of spudcan shape on easing spudcan-footprint interactions, leading to establishment of a novel spudcan shape with a flat base and 4 holes [13] (see inset in Fig. 16a). Without additional mechanical operations in the seabed, it has been shown that this shape can effectively ease spudcan-footprint interaction issues such as a reduction in the induced horizontal force and moment. A footprint with intact soil strength was considered for the development of the shape deliberately to preclude the additional influence of soil strength heterogeneity or to reduce an influential factor [13].

The performance of the novel spudcan installation on the footprint with the remoulded soil strength is assessed here for a more realistic condition. For this analysis, the critical offset distance of β = 1.0D, ET = 1 year and OP = 0 year were selected (Group V in Table 1). The response of the novel spudcan and the generic spudcan are compared in Fig. 16. The vertical resistance (V) of the novel spudcan is approximately 14% lower than that of the generic spudcan (see Fig. 16a). This is mainly due to the (20%) reduced net area and smaller volume under RP of the novel spudcan. However, it is expected that this gap will diminish gradually with the increase of penetration depth as the backfilled soil will cover the spudcan top surface and hence block the soil flow through the holes. All the other response profiles in Figs. 16b~16e show that the novel spudcan shape reduced horizontal force, moment about RP1, lateral displacement and rotation by about 50% relative to the generic spudcan. These results confirm the effectiveness of the novel spudcan on easing spudcan-footprint interactions.

The effectiveness of the novel spudcan is also illustrated by the soil flow mechanisms and the schematic diagram of imbalance force at the depth of H_{max}. The soil flow mechanism graph in inset in Fig. 17a clearly displays the soil flows through the holes of the novel spudcan. Furthermore, the remoulded soil flows through the holes more easily, augmenting the reduction of imbalance force. By comparing Figs. 14c and 17a, it can be seen that the remoulded soil strength contour underneath the spudcan are almost identical for both the

generic and novel spudcans. As such, the lower H_{max} for the novel spudcan also resulted by the flat base of the spudcan. Fig. 17b shows a schematic diagram for the imbalance force on the spudcan bottom. For the generic spudcan, all resistance force vectors are arranged in the left-upper diagonal direction, which generates the additional horizontal force. However, the resistance force vector on the bottom of the novel spudcan only has the vertical directional force component, i.e., no additional horizontal force will be mobilised. In essence, the soil flowing through the holes and the flat base of the novel spudcan has led to ease spudcan-footprint interactions.

The effectiveness of the novel spudcan on the structural integrity of the jack-up leg is shown in Fig. 18, plotting the captured stresses of the structural beam at RP1. The total stress, σ_{Total}, is composed of the normal stress, σ_N and the bending stress, σ_M (see Fig. 18a). The σ_N is induced by the vertical force, V and the σ_M is from the bending moment about RP1, M_t (= M + M_a). At d/D = 0.2 ~ 0.3, the novel spudcan reduced the σ_M by 52 % the σ_{Total} by 41 %. At d/D = 0.6, the reduction in σ_{Total} decreases to ~29 % owing to the reduction in the interaction effect (see Fig. 16) as soil strength becomes closer to the intact strength.

5. CONCLUDING REMARKS

Spudcan penetration on an existing footprint has been investigated through large deformation finite element analyses, accounting for the soil strength that remoulded during creation of the footprint and then regained strength partly during the elapsed time before reinstalling another spudcan. The footprint was set based on the measured strength contour from existing centrifuge test data. A global jack-up rig model was also included, allowing spudcan lateral displacement and rotation to be quantified. The following conclusions can be drawn from the results presented.

1. The maximum horizontal force (H_{max}), moment ($M_{t,max}$), lateral displacement (δ_{Hmax}) and rotation (θ_{max}), all increased by 12~20% and occurred at a deeper depth for the footprint with remoulded soil strength compared to the footprint with intact soil strength.
2. The maximum horizontal force and moment reduced with increasing elapsed time between the creation of the footprint and reinstallation of the spudcan.
3. The critical offset distance of reinstallation of the spudcan from the footprint centre was identified at 0.5~1D.
4. The novel stpudcan shape with a flat base and four holes was shown to reduce horizontal force, moment about RP1, lateral displacement and rotation by about 50%; and total stress on the jack-up leg at RP1 by 41% relative to that obtained with the generic spudcan; confirming the effectiveness of the spudcan shape for easing spudcan-footprint interactions and ensuring structural integrity of the jack-up legs.

The global modelling technique can be used to investigate other offshore structures such as jacket structures, wind turbines. The technique of considering remoulded soil strength contour or true soil conditions around an object can be a very efficient (less time consuming but more precise) for exploring various geotechnical boundary value problems such as the effect of dynamic laying process on the lateral and uplift capacity of pipelines, the effect of installation on capacity of anchors under operational loadings.

6. ACKNOWLEDGEMENTS

The research presented herein was undertaken with support from the Australian Research Council (ARC) through Linkage Project LP140100066. The work forms part of the activities of the Centre for Offshore Foundation Systems (COFS), currently supported as a node of the Australian Research Council Centre of Excellence for Geotechnical Science and Engineering

435 and as a Centre of Excellence by the Lloyd's Register Foundation. This support is gratefully
436 acknowledged, as is the helpful discussion with Dr. Dong Wang.

REFERENCES

[1] J.J. Osborne, Are we good or are we lucky? in: OGP/CORE Workshop, Singapore, 2005.

[2] MSL, Guidelines for jack-up rigs with particular reference to foundation integrity. MSL Engineering Limited for the Health and Safety Executive, Research Report 289, 2004.

[3] C.F. Leung, C.T. Gan, Y.K. Chow, Shear strength changes within jack-up spudcan footprints, in: Proceedings of the 17th International Offshore and Polar Engineering Conference, Lisbon, 2007, pp. 1504-1509.

[4] C.T. Gan, C.F. Leung, M.J. Cassidy, C. Gaudin, Y.K. Chow, Effect of time on spudcan-footprint interaction in clay, Géotechnique 62(5) (2012) 401-413.

[5] C. Gaudin, M.J. Cassidy, T. Donovan, Spudcan reinstallation near existing footprints, in: Proceedings of the 6th International Conference on Offshore Site Investigation and Geotechnics, London, 2007, pp. 285-292.

[6] M.J. Cassidy, C.K. Quah, K.S. Foo, Experimental investigation of the reinstallation of spudcan footings close to exiting footprints, Journal of Geotechnical and Geoenvironmental Engineering, ASCE 135(4) (2009) 474-486.

[7] V.W. Kong, M.J. Cassidy, C. Gaudin, Experimental study of the effect of geometry on reinstallation of jack-up next to footprint, Canadian Geotechnical Journal 50(5) (2013) 557-573.

[8] V.W. Kong, M.J. Cassidy, C. Gaudin, Failure mechanisms of a spudcan penetrating next to an existing footprint, Theoretical and Applied Mechanics Letters 5(2) (2015) 64-68.

[9] M.S. Hossain, R. Stainforth, Perforation drilling for easing spudcan-footprint interaction issues, Ocean Engineering 113 (2016) 308-318.

[10] M.S. Hossain, R. Stainforth, V.T. Ngo, M.J. Cassidy, Y.H. Kim, M.J. Jun, Experimental investigation on the effect of spudcan shape on spudcan-footprint interaction, Applied Ocean Research 69 (2017) 65-75.

[11] W. Zhang, M.J. Cassidy, Y. Tian, 3D large deformation finite element analyses of jack-up reinstallations near idealised footprints, in: Proceedings of the 15th International

Conference on the Jack-up Platform Design, Construction and Operation, London, 2015.

[12] M.J. Jun, Y.H. Kim, M.S. Hossain, M.J. Cassidy, Y. Hu, J.U. Sim, Numerical investigation of novel spudcan shapes for easing spudcan-footprint interactions, Journal of Geotechnical and Geoenvironmental Engineering, ASCE 144(9) (2018) 04018055.

[13] M.J. Jun, Y.H. Kim, M.S. Hossain, M.J. Cassidy, Y. Hu, S.G. Park, Optimising spudcan shape for mitigating spudcan-footprint interaction, Applied Ocean Research 79 (2018) 62-73.

[14] Hartono, K.K. Tho, D.F. Leung, Y.K. Chow, Centrifuge and numerical modelling of reaming as mitigation measure for spudcan-footprint interaction, in: Proceedings of the 2014 Offshore Technology Conference Asia, Kuala Lumpur, 2014, OTC0-24835-MS.

[15] K.K. Tho, N. Chan, Y. Zhou, J. Liu, S. Zhou, Case study of spudcan re-penetration analysis using large deformation finite element approach, in: Proceedings of the 15th International Conference on the Jack-up Platform Design, Construction and Operation, London, 2015.

[16] Z. Chen, K.K. Tho, C.F. Leung, Y.K. Chow, Influence of overburden pressure and soil rigidity on uplift behavior of square plate anchor in uniform clay, Computers and Geotechnics 52 (2013) 71-81.

[17] K.K. Tho, Z. Chen, C.F. Leung, Y.K. Chow, 2013. Pullout behaviour of plate anchor in clay with linearly increasing strength, Canadian Geotechnical Journal 51(1) (2013) 92-102.

[18] O. A. Purwana, C. F. Leung, Y. K. Chow, K. S. Foo, Influence of base suction on extraction of jack-up spudcans, Géotechnique 55(10) (2005) 741–753.

[19] M.S. Hossain, X. Dong, Extraction of spudcan foundations in single and multilayer soils, Journal of Geotechnical and Geoenvironmental Engineering, ASCE 140(1) (2014) 170-184.

[20] M.S. Hossain, J. Zheng, A. Huston, Effect of spudcan geometry on penetration and extraction resistance in clay, Géotechnique 65(2) (2015) 147-154.

[21] M.J. Jun, Y.H. Kim, M.S. Hossain, M.J. Cassidy, Y.Hu, S.G. Park, Global jack-up rig behaviour next to a footprint. Marine Structures 64 (2019) 421-441.

[22] Dassault Systèmes, ABAQUS analysis user's manual, Simulia Corp., Providence, R.I., 2012.

[23] P. Hu, D. Wang, S.A. Stanier, M.J. Cassidy, Assessing the punch-through hazard of a spudcan on sand overlying clay, Géotechnique 65(11) (2015) 883-896.

[24] J. Zheng, M.S. Hossain, D. Wang, New design approach for spudcan penetration in nonuniform clay with an interbedded stiff layer, Journal of Geotechnical and Geoenvironmental Engineering, ASCE 141(4) (2015) 04015003.

[25] G. Qiu, S.Henke, Controlled installation of spudcan foundations on loose sand overlying weak clay, Marine Structures 24(4) (2011) 528–550.

[26] P. Hu, D. Wang, M.J. Cassidy, S.A. Stanier, Predicting the resistance profile of a spudcan penetrating sand overlying clay, Canadian Geotechnical Journal 51(10) (2014) 1151-1164.

[27] K. K. Tho, C. F. Leung, Y. K. Chow, S. Swaddiwudhipong, Eulerian finite element technique for analysis of jack-up spudcan penetration, International Journal of Geomechanics 12(1) (2012) 64–73.

[28] J. Zheng, M. S. Hossain, D. Wang, Numerical investigation of spudcan penetration in multi-layer deposits with an interbedded sand layer, Geotechnique 67(12) (2017)1050-1066.

[29] I. Einav, M.F. Randolph, Combining upper bound and strain path methods for evaluating penetration resistance, International Journal of Numerical Methods in Engineering 63(14) (2005) 1991-2016.

[30] M. S. Hossain, M.F. Randolph, Effect of strain rate and strain softening on the penetration resistance of spudcan foundations on clay, International Journal of Geomechanics 9(3) (2009) 122-132.

[31] Y.H. Kim, M.S. Hossain, Dynamic installation, keying and diving of OMNI-Max anchors in clay, Géotechnique 67(1) (2017) 78-85.

[32] J. Ma, D. Wang, M.F. Randolph, A new contact algorithm in the material point method for geotechnical simulation, International Journal for Numerical and Analytical Methods in Geomechanics 38 (2014) 1197-1210.

[33] Y.H. Kim, M.S. Hossain, Dynamic installation of OMNI-Max anchors in clay: Numerical Analysis, Géotechnique 65(12) (2015) 1029-1037.

[34] D. Wang, B. Bienen, M.Nazem, Y.Tian, J. Zheng, T. Pucker, M.F. Randolph, Large deformation finite element analyses in geotechnical engineering, Computers and Geotechnics 65 (2015) 104-114.

[35] D.F. Mao, M.H. Zhang, Y. Yu, M.L. Duan, J. Zhao, Analysis of spudcan-footprint interaction in a single soil with nonlinear FEM, Petroleum Science 12(1) (2015) 148-156.

[36] N. Wang, J. Wu, Y. Xu, Z. Huang, L. Zhu, Research on soil failure modes and spudcan penetration depths in a single layer, In Proceedings of the 22nd International Offshore and Polar Engineering Conference, Rhodes, 2012, 2, pp. 700-704.

[37] International Organization for Standardization (ISO), Petroleum natural gas industries – Site specific assessment of mobile offshore units – Part 1: Jack-ups, ISO 19905-1, 2012.

[38] InSafeJIP, Improved guidelines for the prediction of geotechnical performance of spudcan foundations during installation and removal of jack-up units. Joint Industry Funded Project, 2011.

[39] Y. Zhao, H. Liu, P. Li, An efficient approach to incorporate anchor line effects into the coupled Eulerian-Lagrangian analysis of comprehensive anchor behaviors. Applied Ocean Research 59 (2016) 201-215.

[40] D. Menzies, R. Roper, Comparison of jackup rig spudcan penetration methods in clay. in: Proceedings of the 40th offshore technology conference, Houston, paper OTC 19545, 2008.

548 [41] D.P. Stewart, I.M.S. Finnie, Spudcan-footprint interaction during jack-up workovers, in:
549 Proceedings of the 11th international offshore and polar engineering conference,
550 Stavanger, 2001, pp. 61-65.

551 [42] C.T. Gan, Centrifuge model study on spudcan-footprint interaction, Ph.D. thesis,
552 National University of Singapore, 2009.

553 [43] Hartono, Centrifuge model study on spudcan-footprint remediation techniques, Ph.D.
554 thesis, National University of Singapore, 2014.

555 [44] R.J. Jardine, N. Kovecevic, M.J.R. Hoyle, H.K. Sidhu, A. Letty, A study of eccentric
556 jack-up penetration into infilled footprint craters, in: Proceedings of the 8th
557 International Conference on the Jack-up Platform Design, Construction and Operation,
558 London, 2001.

559 [45] R.J. Jardine, N. Kovacevic, M.J.R. Hoyle, H.K. Sidhu, A. Letty, Assessing the effects on
560 jack up structures of eccentric installation over infilled craters, in: Proceedings of
561 International Conference on Offshore Site Investigation and Geotechnics, London,
562 2002, pp. 307-324.

563 [46] A. Grammatikopoulou, R.J. Jardine, N. Kovacevic, D.M. Potts, D.M. Hoyle, K.M.
564 Hampson, Potential solutions to the problem of the eccentric installation of jack-up
565 structures into old footprint craters, in: Proceedings of International Conference on
566 Offshore Site Investigation and Geotechnics, London, 2007, pp. 293-300.

567 [47] Hartono, D.F. Leung, K.K. Tho, Y.K. Chow, Reaming as mitigation measure for jack-up
568 reinstallation close to existing footprint, in: Proceedings of the 14th International
569 Conference on the Jack-up Platform Design, Construction and Operation, London,
570 2013.

571 [48] P. Handidjaja, C.T. Gan, C.F. Leung, Y.K. Chow, Jack-up foundation performance over
572 spudcan footprints analysis of a case history, in: Proceedings of the 12th International
573 Conference on the Jack-up Platform Design, Construction and Operation, London,
574 2009.

575

576 Nomenclature

$A_{hull\ bottom}$	bottom area of jack-up rig hull
$A_{\delta Rsu}$	area of δR_{su}
c_d	dilatational wave speed of the material
D	spudcan diameter at largest section
D_{field}	prototype spudcan diameter
D_h	hole diameter
D_{LDFE}	spudcan diameter in LDFE
d	penetration depth of spudcan base
d_e	initial penetration depth
d_{Hmax}/D	normalised penetration depth where the maximum horizontal force occurs
ET	elapsed time
e	vertical force eccentricity
e_{Mmax}	eccentricity at maximum moment
e_{leg}	leg eccentricity
F_{imb}	imbalance force induced by δR_{su}
g	acceleration of gravity
H	horizontal force at spudcan base level
H_{max}	maximum horizontal force at spudcan base level
$H_{max,\beta max}$	largest H_{max} among the various offset distances
K_{buoy}	spring stiffness of buoyancy
K_V, K_H and K_M	initial vertical, horizontal and moment foundation stiffness calculated by LDFE analysis
L_H	horizontal location of remoulded soil strength mapping
L_{leg}	leg length of a jack-up rig
L_{min}	minimum element dimension in the Eulerian meshes
L_V	vertical location of remoulded soil strength mapping
M (= M_{RP})	moment at spudcan base level
M_a	additional bending moment at RP1
M_{max}	maximum moment at spudcan base level
M_t	moment at leg top

$M_{t,max}$	maximum moment at leg top
OP	operating time
RP	reference point that is the intersection point of the centre line and largest cross section of the spudcan (see Fig. 1)
RP1	reference point at leg just below jack-up rig hull (see Fig. 9)
R_{su}	remoulded soil ratio
S_t	soil sensitivity
s_u	undrained shear strength
$s_{u,ref}$	reference undrained shear strength
$s_{u,remoulded}$	remoulded undrained shear strength
V	vertical force
v_{field}	spudcan penetration rate in field
v_{LDFE}	spudcan penetration rate in LDFE
z	penetration depth below soil surface
α	friction ratio
α_b	spudcan base angle
β	distance between the footprint centre and spudcan centre
Δt	time increment
Δt_N	notional time increment
$\Delta t_{critical}$	critical time increment
$\Delta\varepsilon_1$ & $\Delta\varepsilon_3$	shear strain
δ_H & δ_{Hmax}	spudcan lateral displacement at RP and maximum lateral displacement
δR_{su}	difference of remoulded soil ratio
δ_{LDFE}	specified displacement for each time increment
δ_{rem}	remoulded strength ratio
$\dot{\gamma}$	shear strain rate
$\dot{\gamma}_{ref}$	reference shear strain rate
μ	rate parameter for logarithmic expression
μ_C	Coulomb friction coefficient
θ & θ_{max}	spudcan rotation at RP and maximum rotation

ρ_{sea}	density of sea water
σ_{Total}	structural total stress (= $\sigma_V + \sigma_M$)
σ_M	structural bending stress
σ_N	structural normal stress
τ_{max}	maximum shear stress
ξ	cumulative plastic shear strain
ξ_{95}	cumulative plastic shear strain required for 95% remoulding

577

578 Table 1. Summary of 3D LDFE analysis cases

	Spudcan shape	$s_{u,ref}$ (kPa)	Applied time		s_u mapping	Boundary condition	Offset distance, β (m)	H_{max} (MN)	M_{max} at RP (MN-m)	$M_{t,max}$ at RP1 (MN-m)	Note
			OP (years)	ET (years)							
Validation	Mod V "A" class model spudcan	5.0 + 1.8z	0	1	- (Test result)	Fixed head	0.5D	0.82	15.50	-	Validation case
					Detailed mapping			0.95	15.30		
					Simplified mapping			1.00	16.80		
						Global jack-up rig		0.87	15.1		
Group I	Generic		-		Intact soil			0.89	18.50	-129.2	Effect of remoulded soil
			0	1	Simplified mapping			1.02	17.70	-145.2	
Group II	Generic			100	Simplified mapping			0.91	13.70	-130.9	Effect of time
Group III	Generic			1	Simplified mapping		0.25D	0.69	11.50	-101.5	Effect of offset distance
							0.75D	1.27	18.60	-180.8	
							1.00D	1.31	15.70	-189.9	
							1.25D	0.99	12.30	-143.6	
Group IV	Novel			1			1.00D	0.66 (48.2%)	14.20 (9.6%)	-88.9 (53.2%)	Effect of novel spudcan

579

580

581

582

Submitted Aug. 2019;
Resubmitted Nov. 2019; Re-resubmitted Mar. 2020

Table 2. Information for previous studies - spudcan shape and $s_{u,ref}$ profile

Reference	Spudcan shape	Initial penetration depth, d_e	$s_{u,ref}$ (intact condition)
Cassidy et al. [6]	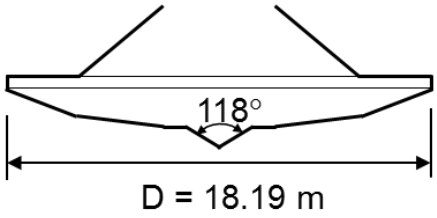	5.67 m (= 0.31D)	7.5 + 2.0z (kPa)
Zhang et al. [11]	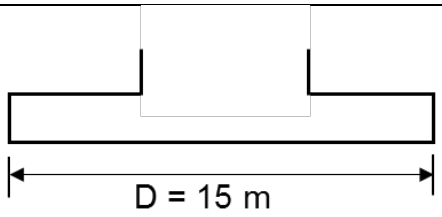	- (artificial footprint)	7.5 + 0.92z (kPa) z < 3.4 m 5.0 + 1.68z (kPa) z ≥ 3.4 m
Stewart and Finnie [41]	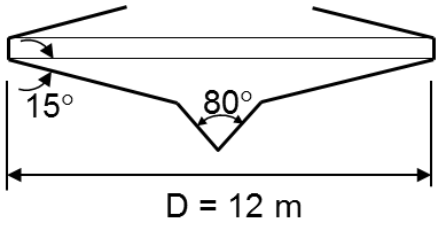	6.48 m (= 0.54D)	12.0 + 2.65z (kPa)
Gan [42]	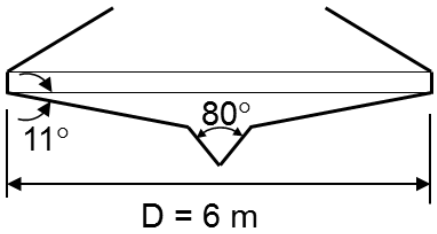	5.19 ~ 5.61 m (= 0.87D ~ 0.94D)	28.0 + 5.0z (kPa)
Hartono [43]	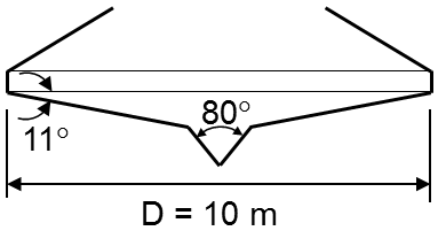	4.71 m (= 0.47D)	$17.0z^{0.55}$ (kPa)

Submitted Aug. 2019;
Resubmitted Nov. 2019; Re-resubmitted Mar. 2020

No. of Figs.: 17

Fig. 1. Typical mesh used in 3D LDFE: (a) typical mesh; (b) detail plan view; (c) detail section view

Fig. 2. Spudcan, soil and jack-up rig global model

Fig. 3. R_{su} map from centrifuge test (after Gan et al. [4])

Fig. 4. Soil model for the detailed and simplified mapping of a footprint with remoulded soil, an operating time of 0.0 years and an elapsed time of 1.0 year: (a) modification of the R_{su} map for LDFE analysis (detailed mapping); (b) modification of the R_{su} map for LDFE analysis (simplified mapping); (c) detailed and simplified mapping to the soil model

Fig. 5. Validation analysis against centrifuge test results: (a) vertical resistance force; (b) horizontal resistance force; (c) moment resistance; (d) lateral displacement; (e) rotation; (f) FE models

Fig. 6. Responses for footprints with intact soil vs remoulded soil: (a) vertical resistance force; (b) horizontal resistance force; (c) moment resistance; (d) eccentricity; (e) lateral displacement; (f) rotation

Fig. 7. Schematic diagram for the imbalance force, F_{imb}, induced by different soil strengths, δRsu, between the left and right side of the spudcan: (a) difference in R_{su}, δR_{su} and area of $A\delta_{Rsu}$ (b) imbalance force induced by δR_{su}

Fig. 8. Failure mechanism, contour line for soil strength and schematic diagram of the imbalance force with spudcan penetration depth: (a) d_{Hmax}/D = 0.065 (H_{max} = penetration depth of the footprint with intact soil); (b) d_{Hmax}/D = 0.338 (H_{max} = penetration depth of the footprint with remoulded soil); (c) d/D = 0.50

Fig. 9. Moment at RP and RP1: (a) moment difference at RP and RP1; (b) moment at RP and RP1

Fig. 10. Soil model for detailed and simplified mapping of a footprint with remoulded soil, operating time of 0.0 years and elapsed time of 100 years: (a) R_{su} map from centrifuge test (after Gan et al., 2012); (b) modification for LDFE analysis (simplified mapping); (c) mapping to LDFE model

Submitted Aug. 2019;
Resubmitted Nov. 2019; Re-resubmitted Mar. 2020

Submitted Aug. 2019;
Resubmitted Nov. 2019; Re-resubmitted Mar. 2020

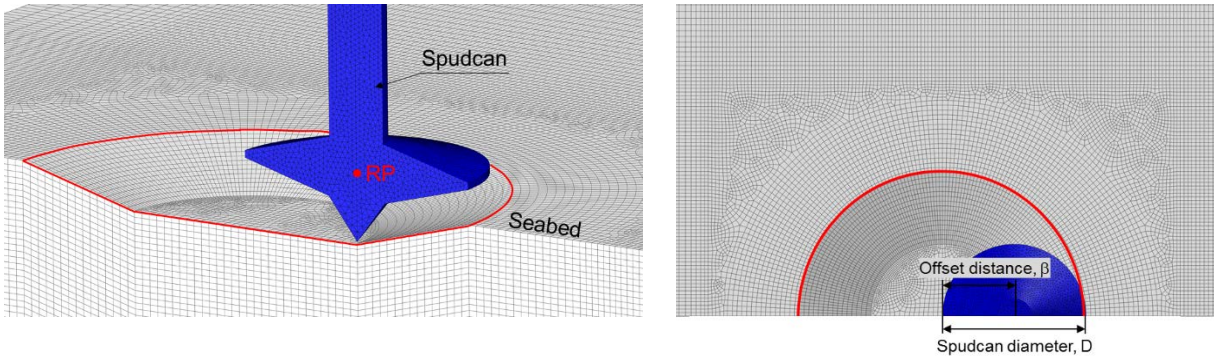

(a) Typical mesh (b) Detail plan view

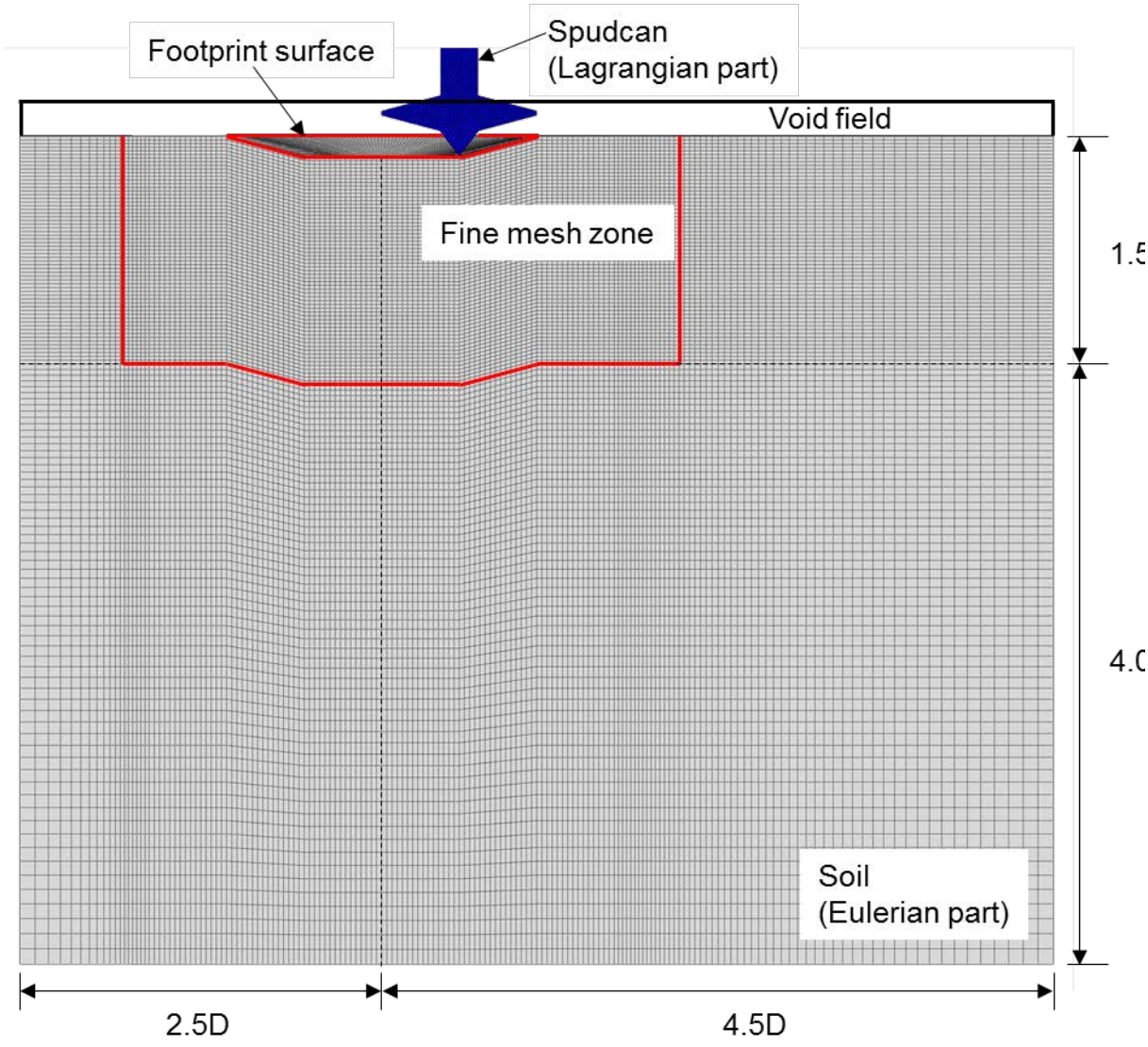

(c) Detail section view

Fig. 1. Typical mesh used in 3D LDFE

Submitted Aug. 2019;
Resubmitted Nov. 2019; Re-resubmitted Mar. 2020

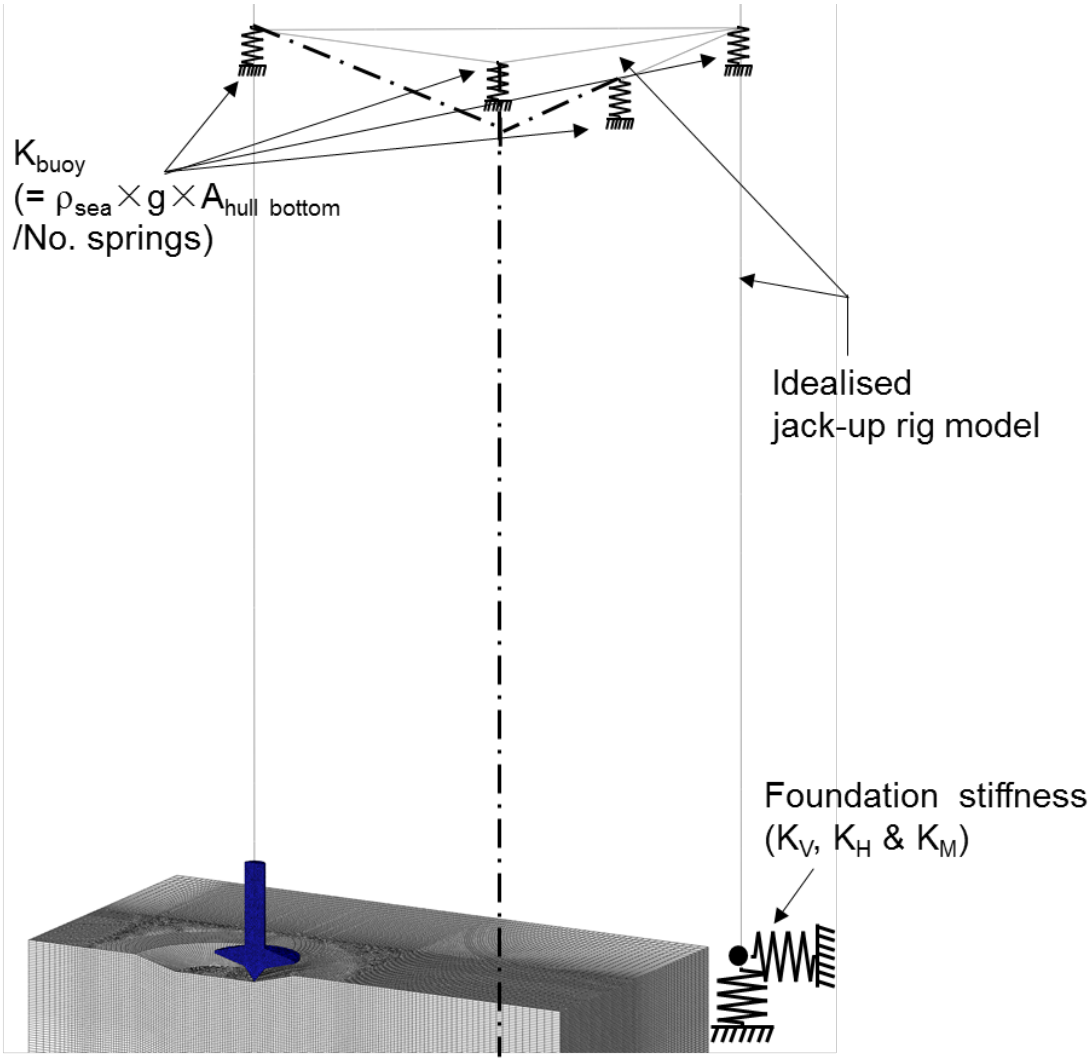

Fig.2. Spudcan, soil and jack-up rig global model

Submitted Aug. 2019;
Resubmitted Nov. 2019; Re-resubmitted Mar. 2020

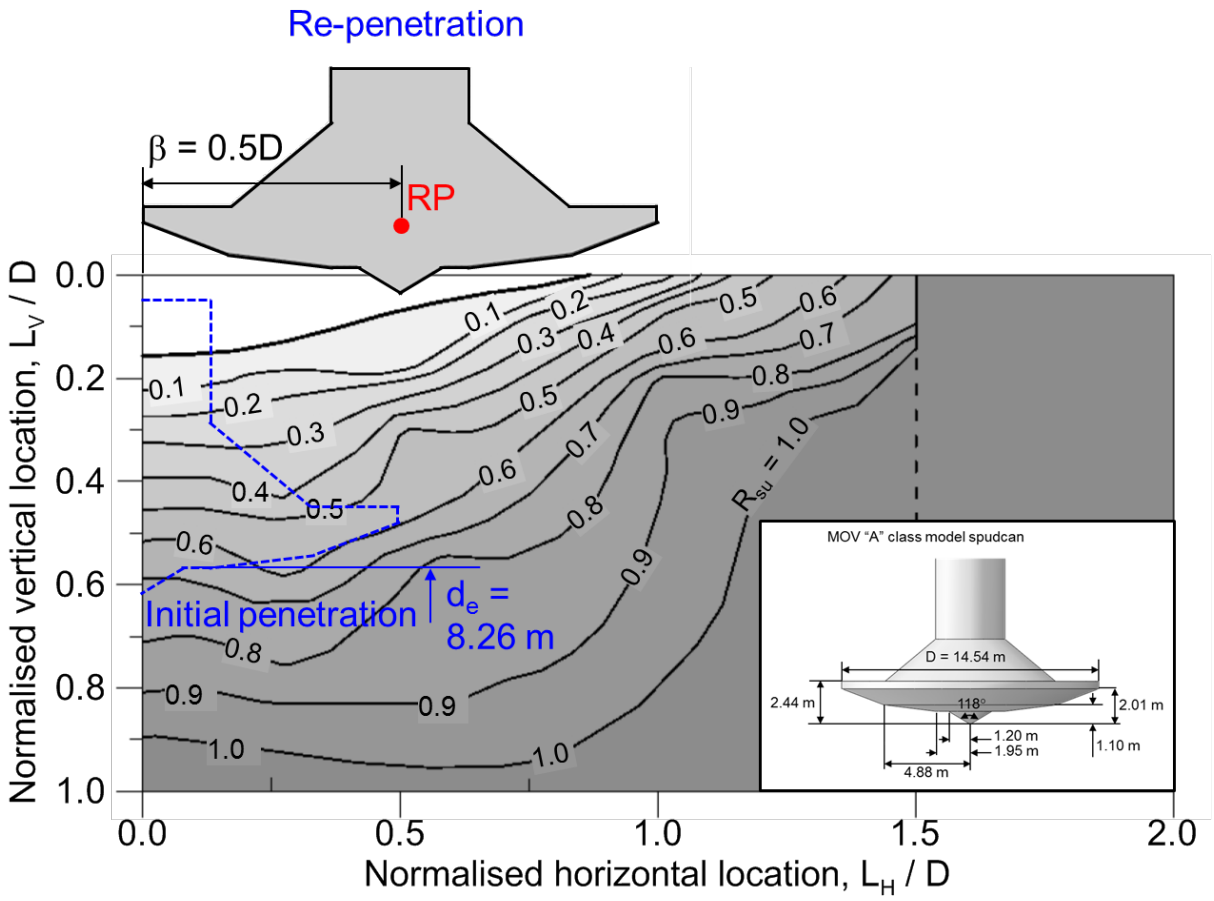

Fig. 3. R_{su} map from centrifuge test (after Gan et al. [4])

Submitted Aug. 2019;
Resubmitted Nov. 2019; Re-resubmitted Mar. 2020

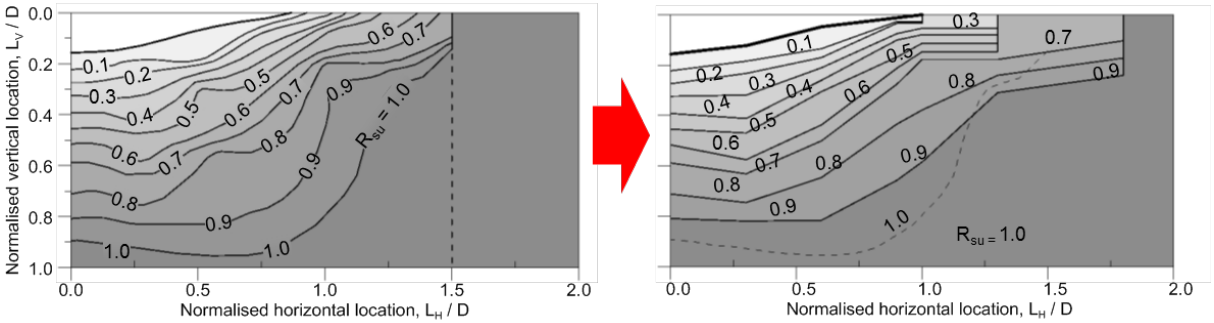

(a) Modification of R_{su} map for LDFE analysis (detailed mapping)

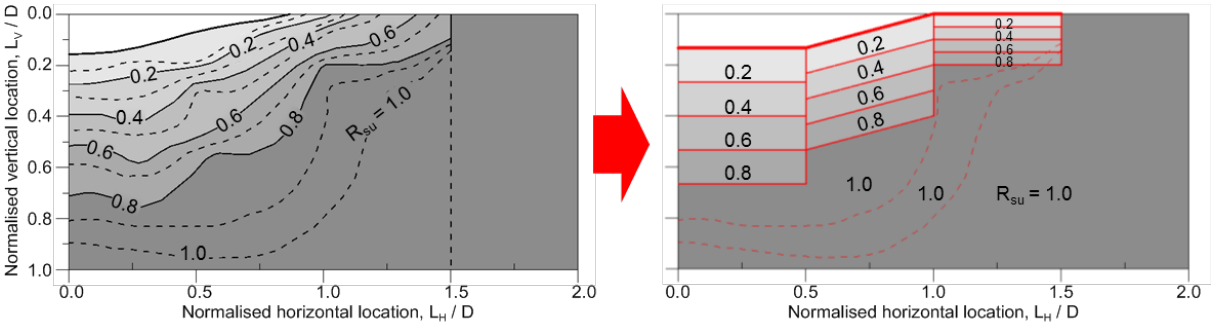

(b) Modification of R_{su} map for LDFE analysis (simplified mapping)

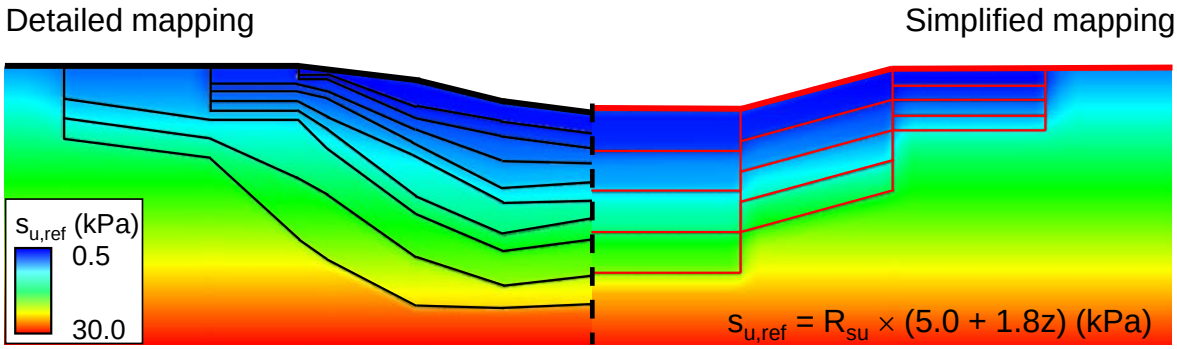

(c) Detailed and simplified mapping to the soil model

Fig. 4. Soil model for the detailed and simplified mapping of a footprint with remoulded soil, an operating time of 0.0 years and an elapsed time of 1.0 year

Submitted Aug. 2019;
Resubmitted Nov. 2019; Re-resubmitted Mar. 2020

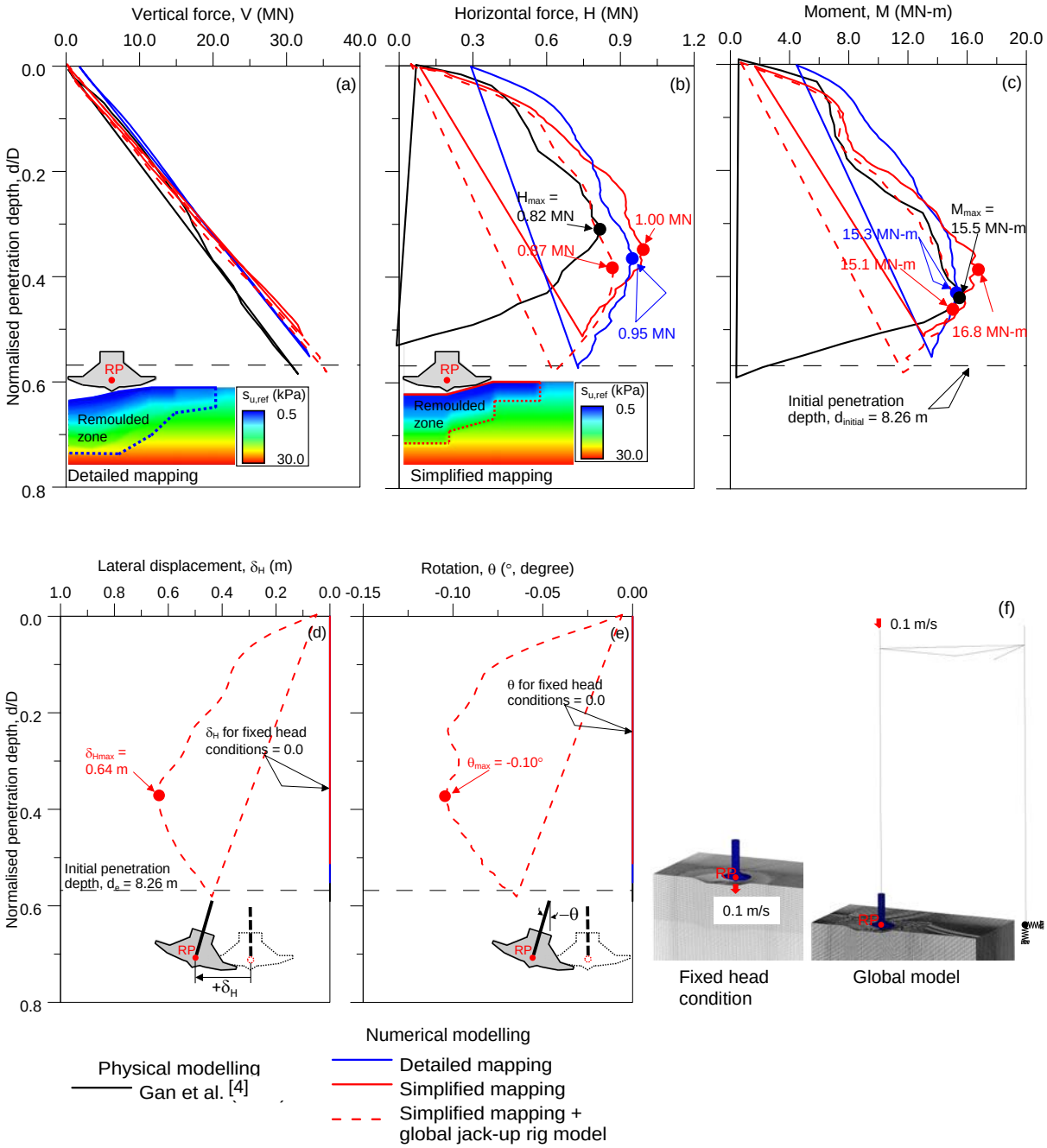

Fig. 5. Validation analysis against centrifuge test results: (a) vertical resistance force; (b) horizontal resistance force; (c) moment resistance; (d) lateral displacement; (e) rotation; (f) FE models

Submitted Aug. 2019;
Resubmitted Nov. 2019; Re-resubmitted Mar. 2020

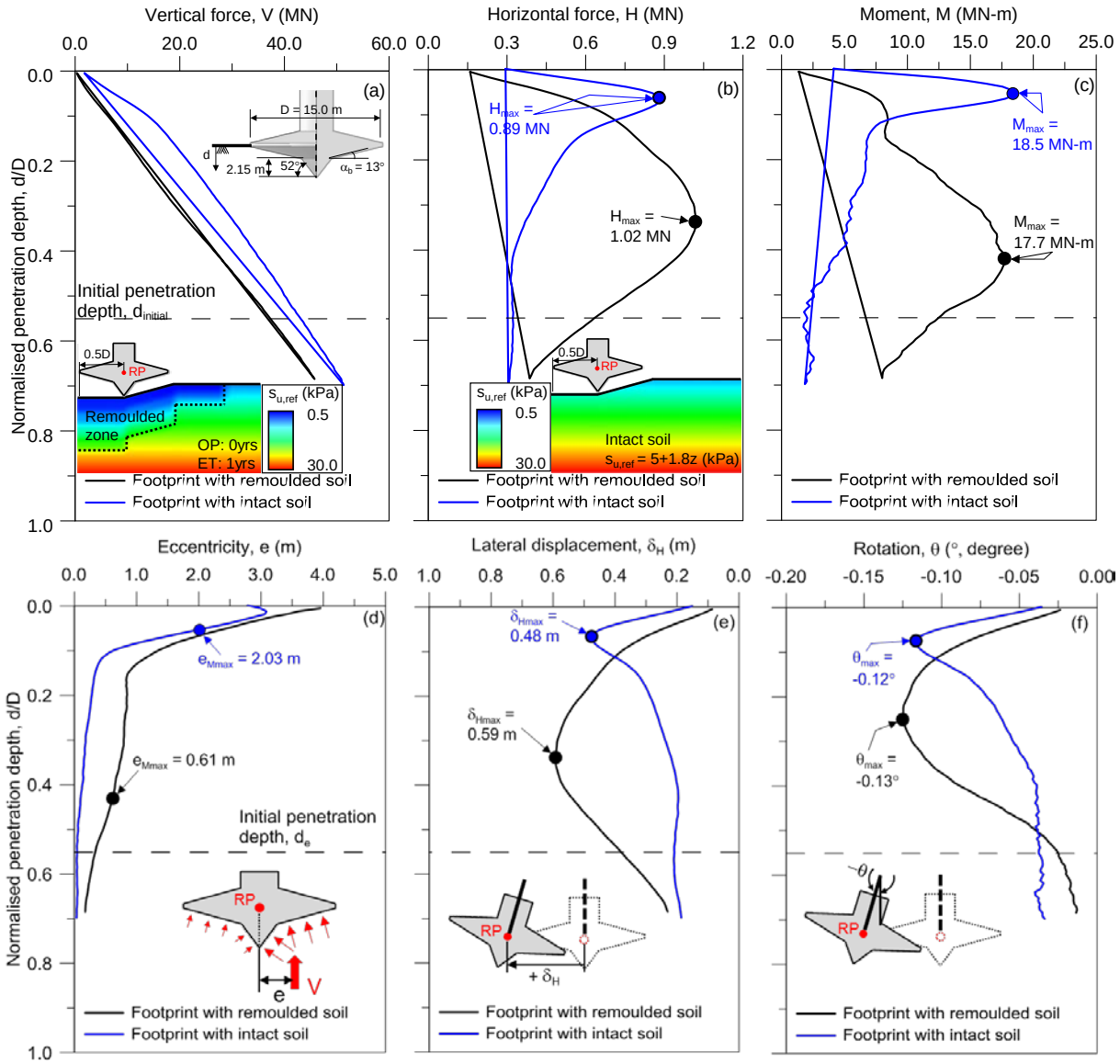

Fig. 6. Responses for footprints with intact soil vs remoulded soil: (a) vertical resistance force; (b) horizontal resistance force; (c) moment resistance; (d) eccentricity; (e) lateral displacement; (f) rotation

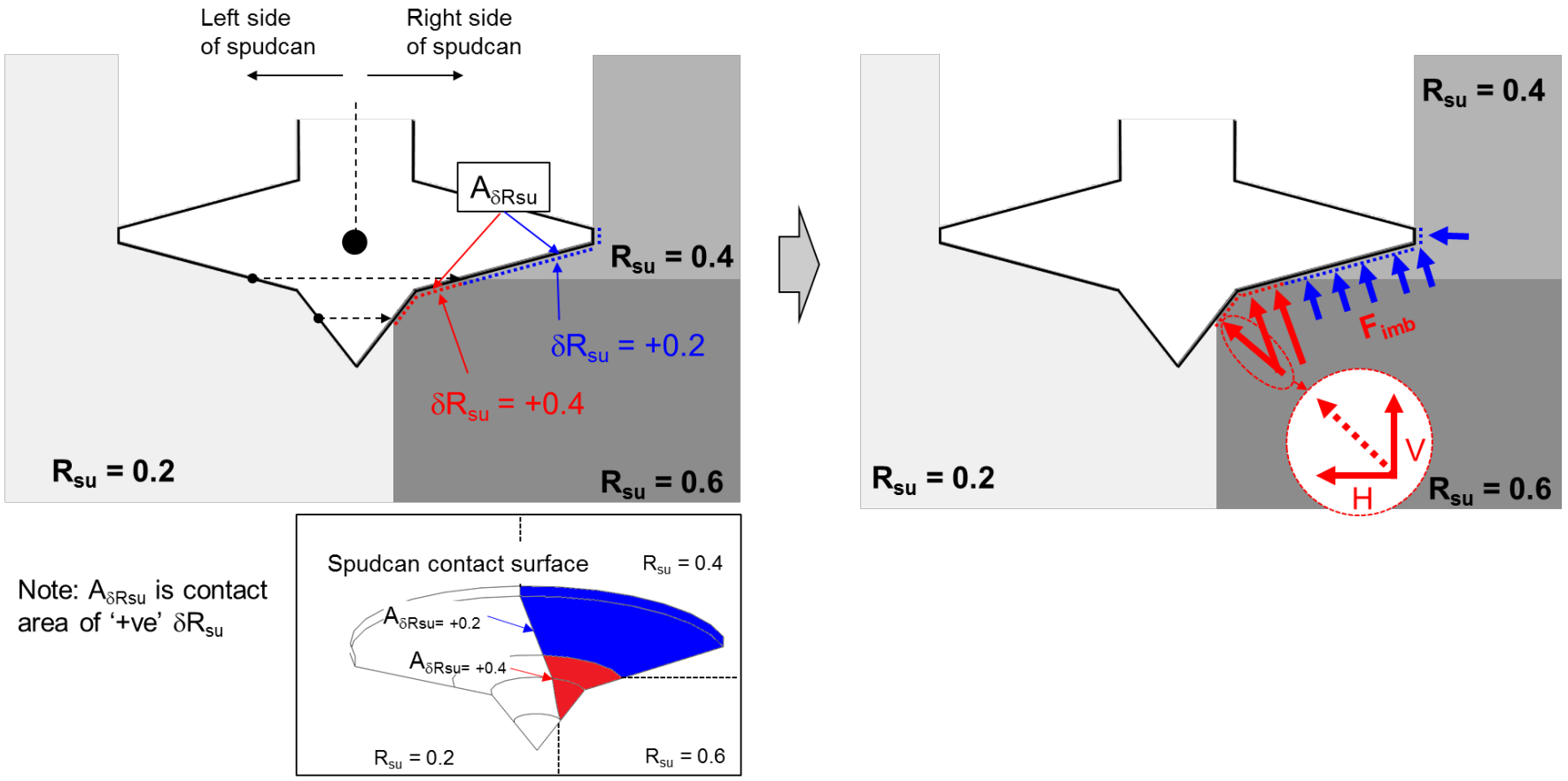

(a) Difference R_{su}, δR_{su} and area of $A_{\delta Rsu}$ (b) Imbalance force induced by δR_{su}

Fig. 7. Schematic diagram for imbalance force, F_{imb}, induced by different soil strength, δR_{su}, between the left and right side of the spudcan

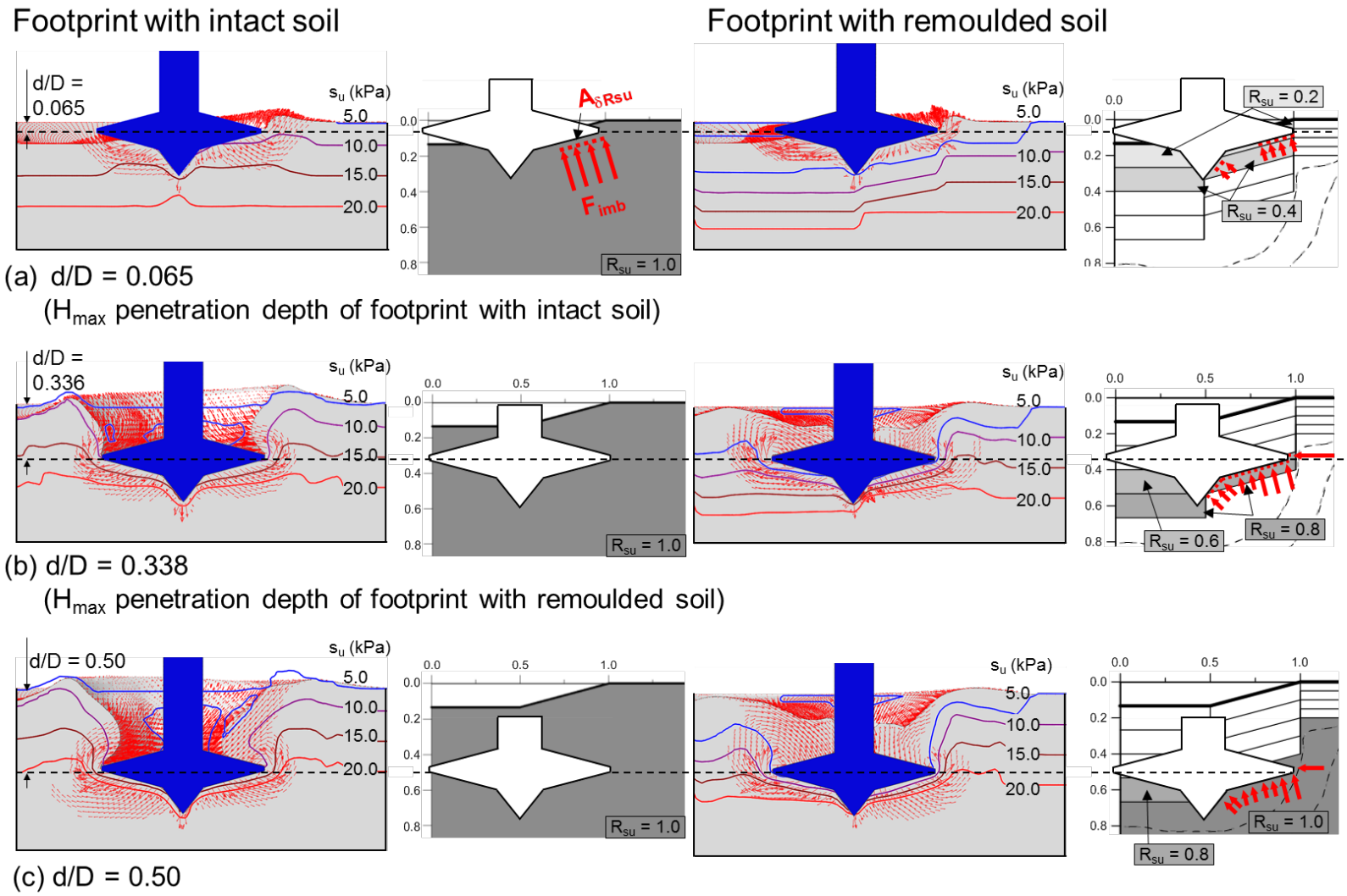

Fig. 8. Failure mechanism, contour line for soil strength and schematic diagram of imbalance force with spudcan penetration depth

Submitted Aug. 2019;
Resubmitted Nov. 2019; Re-resubmitted Mar. 2020

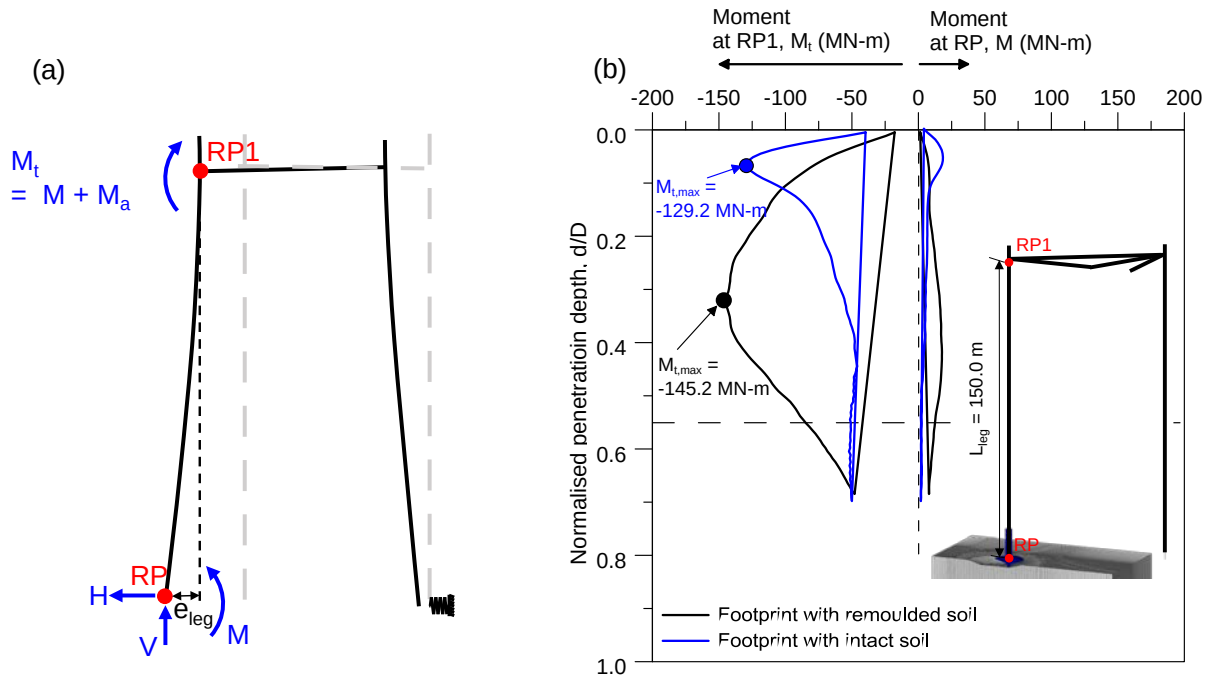

Fig. 9. Moment at RP and RP1: (a) moment difference at RP and RP1; (b) moment at RP and RP1

Submitted Aug. 2019;
Resubmitted Nov. 2019; Re-resubmitted Mar. 2020

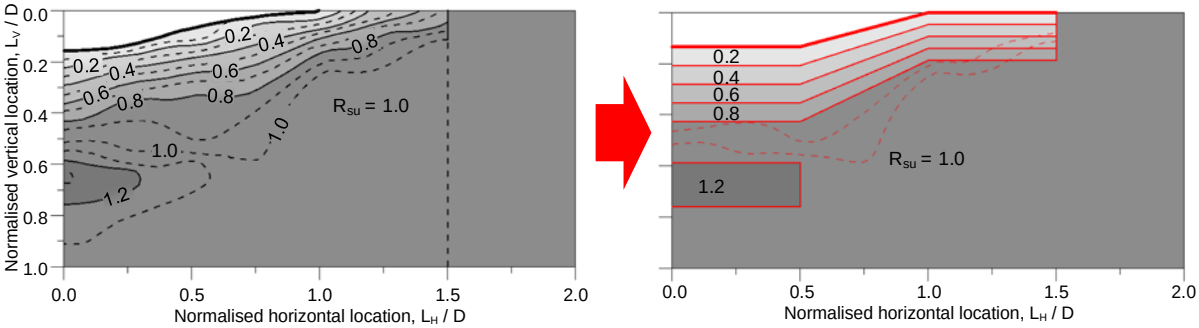

(a) R_{su} map from centrifuge map (after Gan et al. [4])

(b) Modification of R_{su} map for LDFE analysis (simplified mapping)

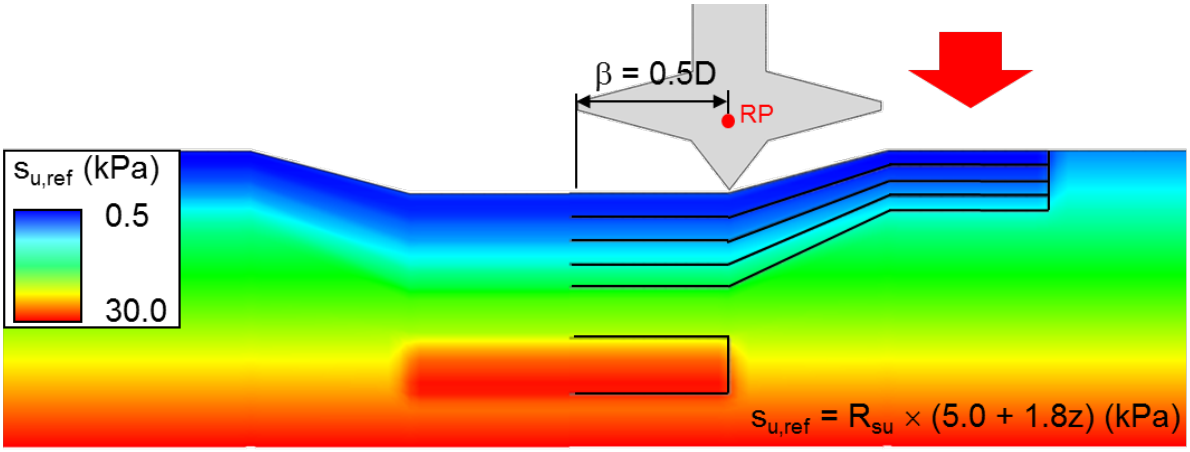

(c) Mapping to LDFE model

Fig. 10. Soil model for detailed and simplified mapping for a footprint with remoulded soil, operating time of 0.0 year and elapsed time of 100 years

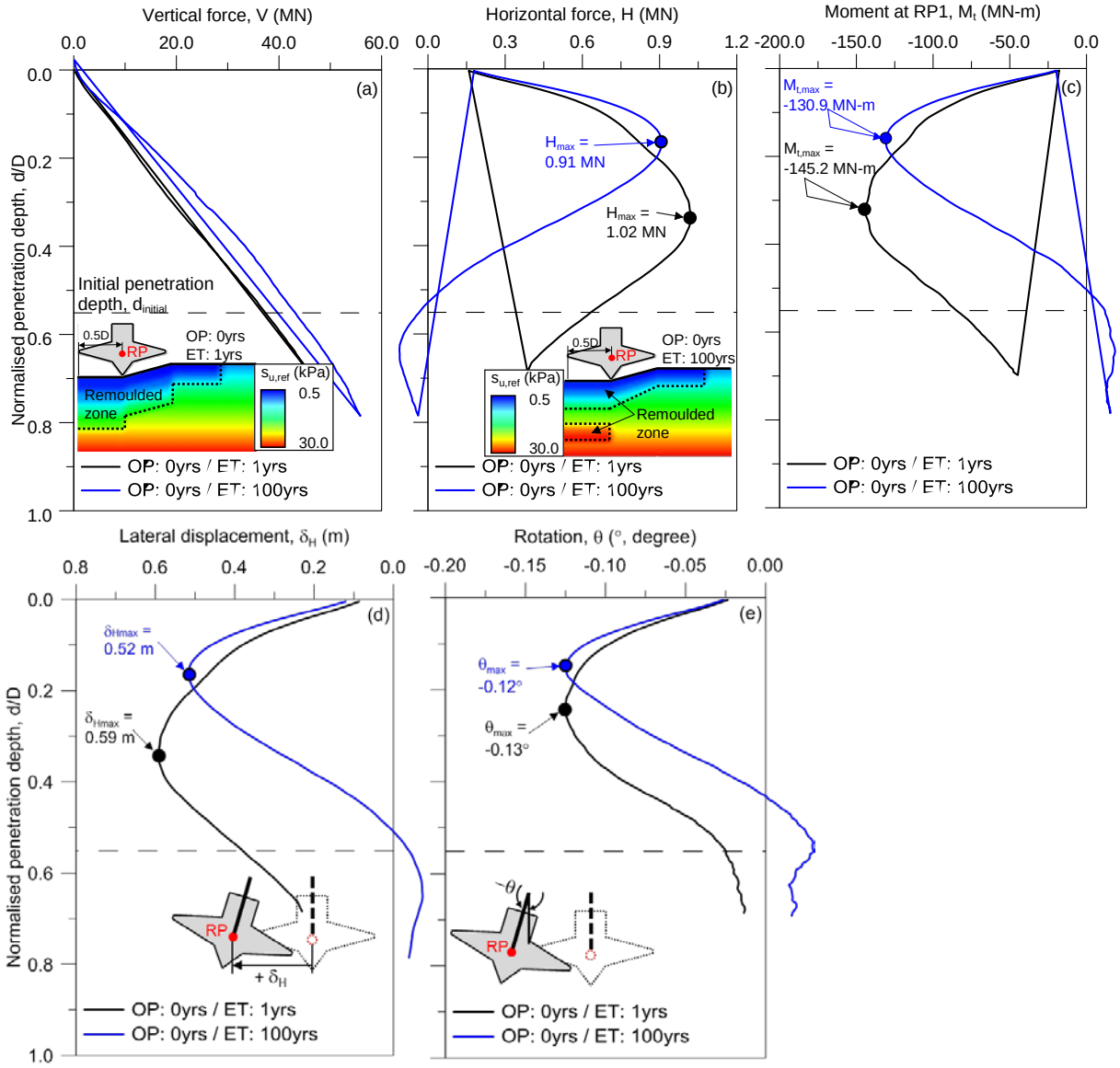

Fig. 11. Responses for different elapsed time (ET: 1 year vs 100 years) : (a) vertical resistance force; (b) horizontal resistance force; (c) moment resistance at RP1; (d) lateral displacement; (e) rotation

Submitted Aug. 2019;
Resubmitted Nov. 2019; Re-resubmitted Mar. 2020

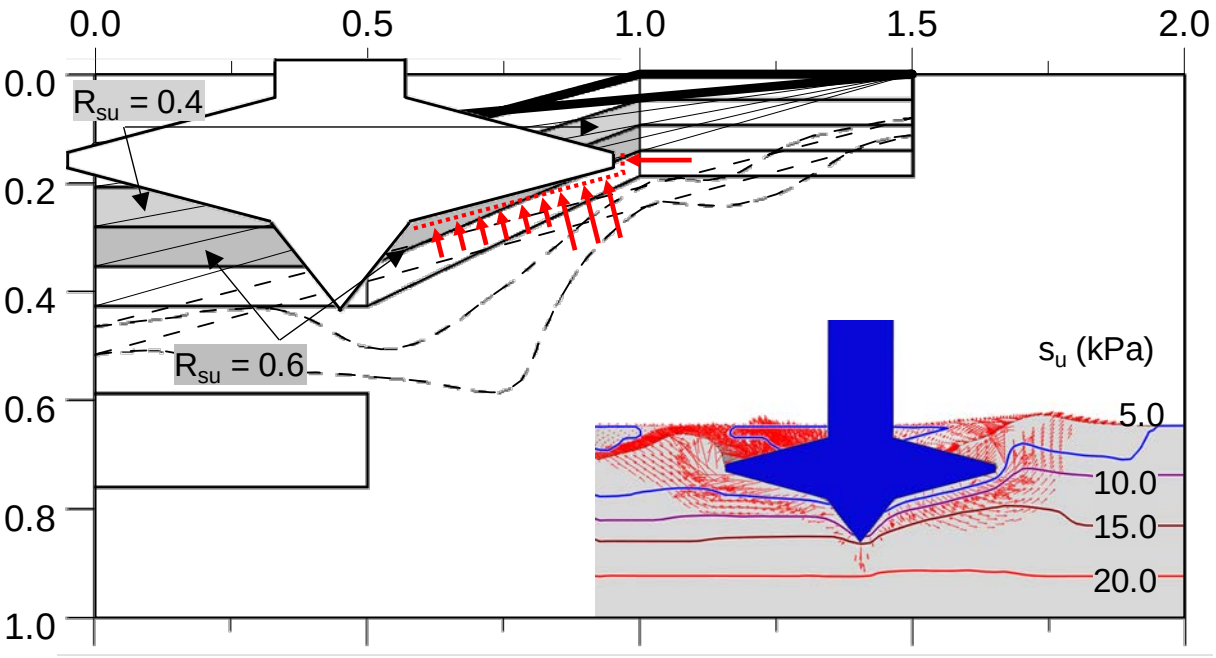

Fig. 12. Schematic diagram of imbalance force, failure mechanism and contour line for soil strength (ET: 100 years)

Submitted Aug. 2019;
Resubmitted Nov. 2019; Re-resubmitted Mar. 2020

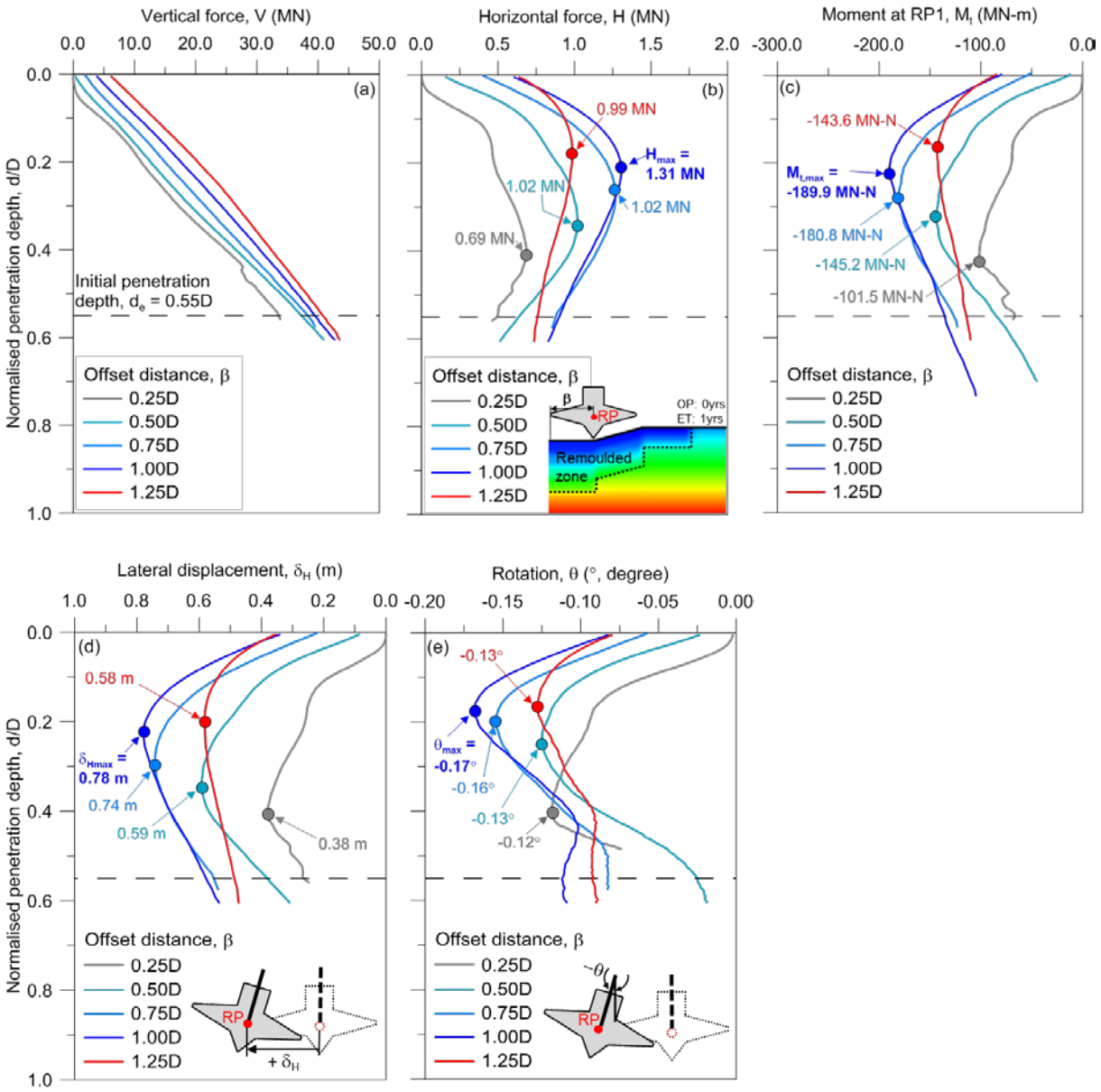

Fig. 13. Responses for different offset distances (β = 0.25D, 0.50D, 0.75D, 1.00D and 1.25D): (a) vertical resistance force; (b) horizontal resistance force; (c) moment resistance; (d) lateral displacement; (e) rotation

Submitted Aug. 2019;
Resubmitted Nov. 2019; Re-resubmitted Mar. 2020

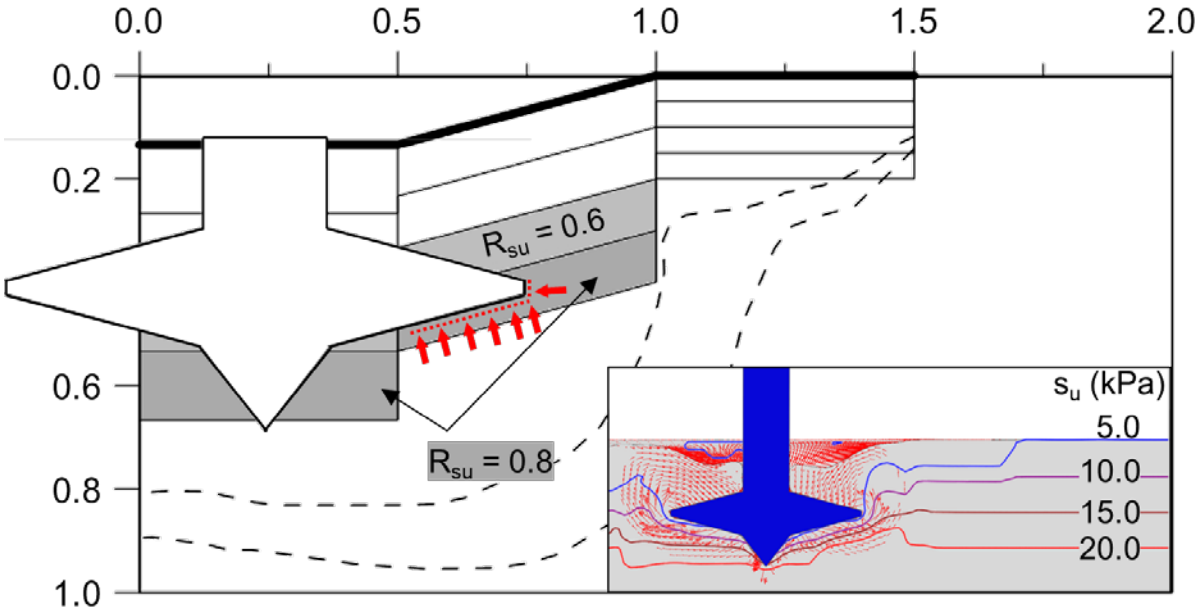

(a) β = 0.25D; d_{Hmax}/D = 0.40

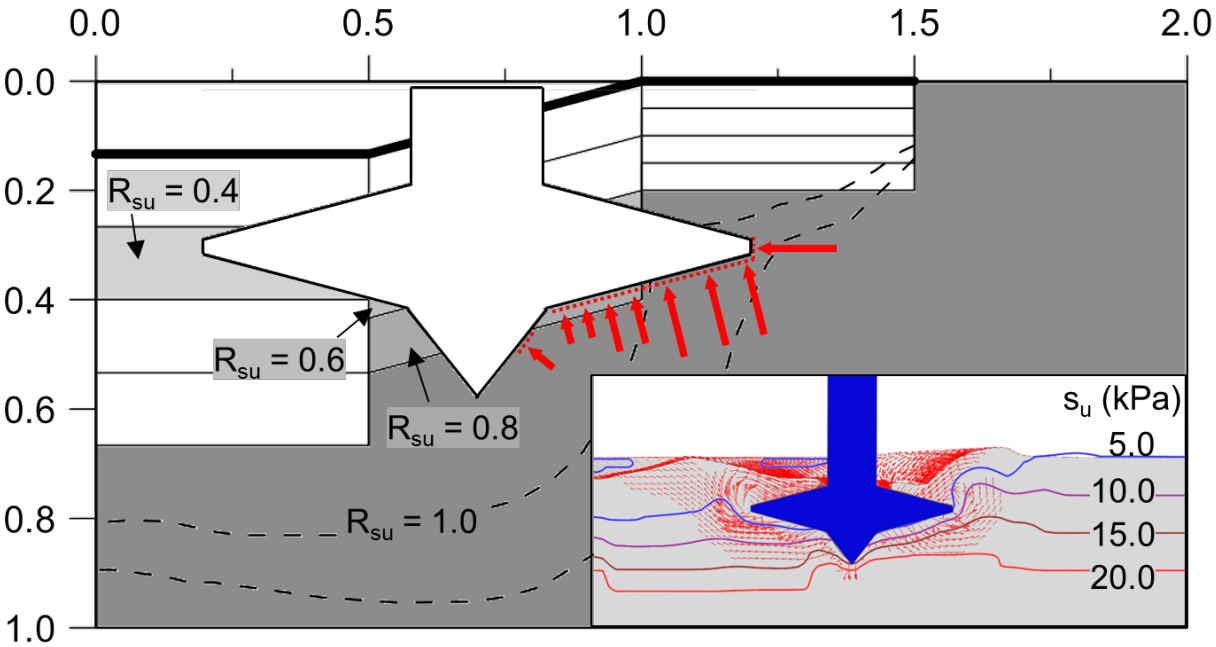

(b) β = 0.75D; d_{Hmax}/D = 0.27

Submitted Aug. 2019;
Resubmitted Nov. 2019; Re-resubmitted Mar. 2020

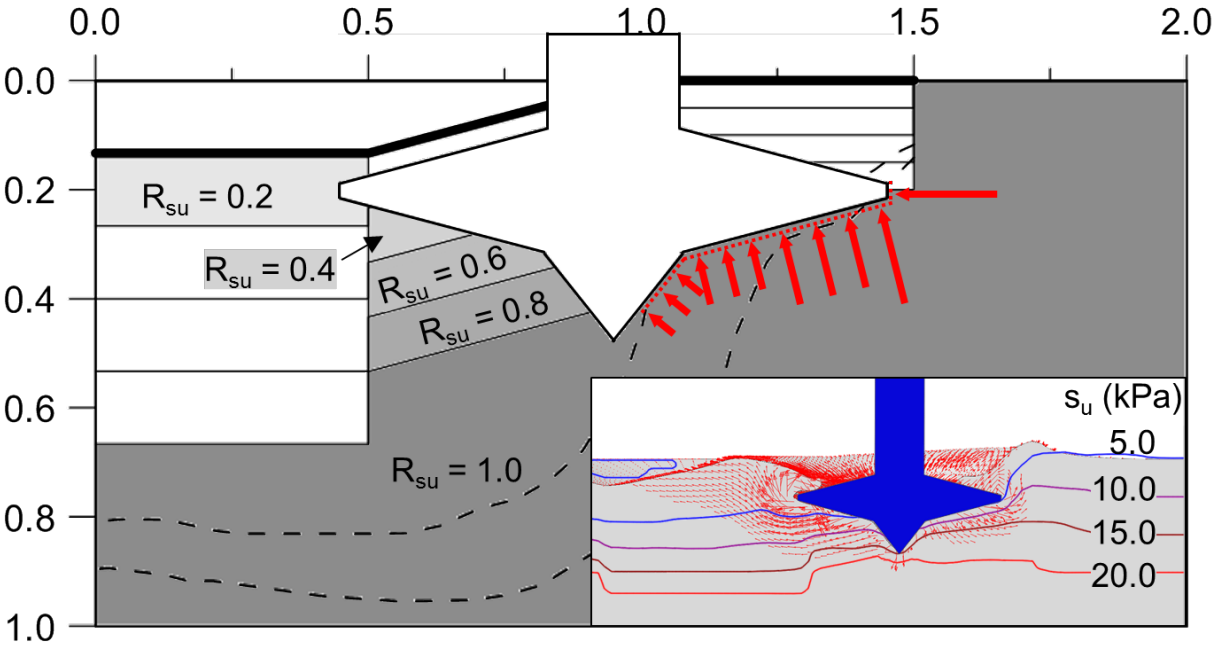

(c) β = 1.00D; d_{Hmax}/D = 0.21

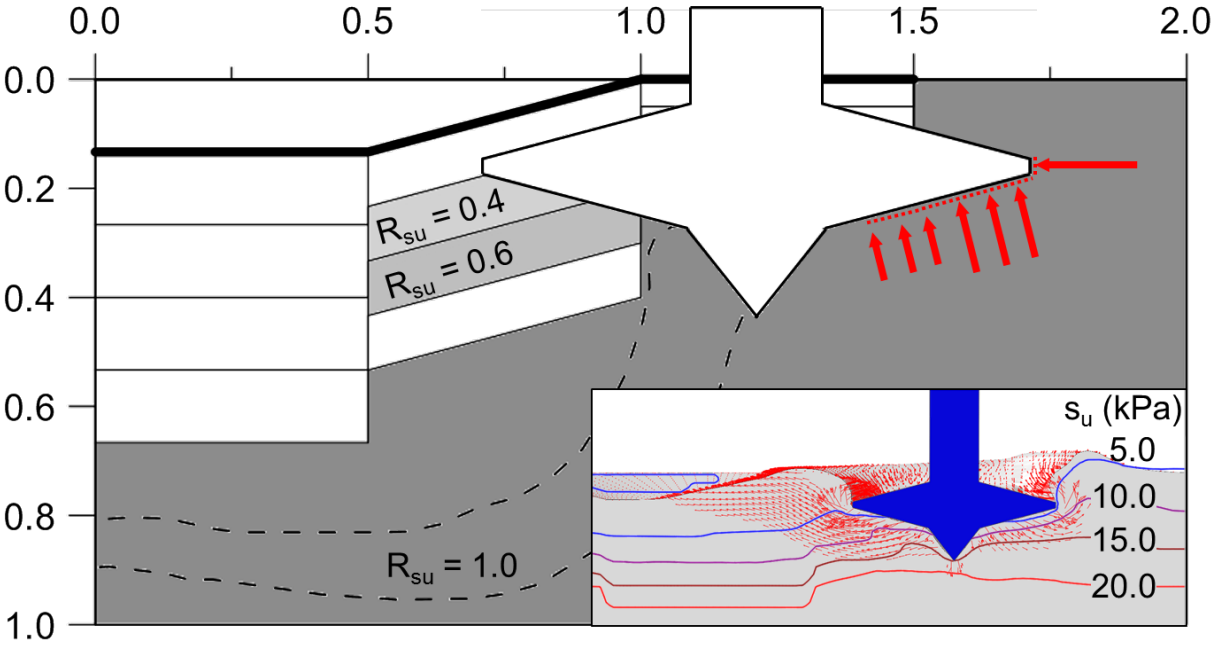

(d) β = 1.25D; d_{Hmax}/D = 0.18

Fig. 14. Schematic diagram of imbalance force, failure mechanism and contour line for soil strength

Submitted Aug. 2019;
Resubmitted Nov. 2019; Re-resubmitted Mar. 2020

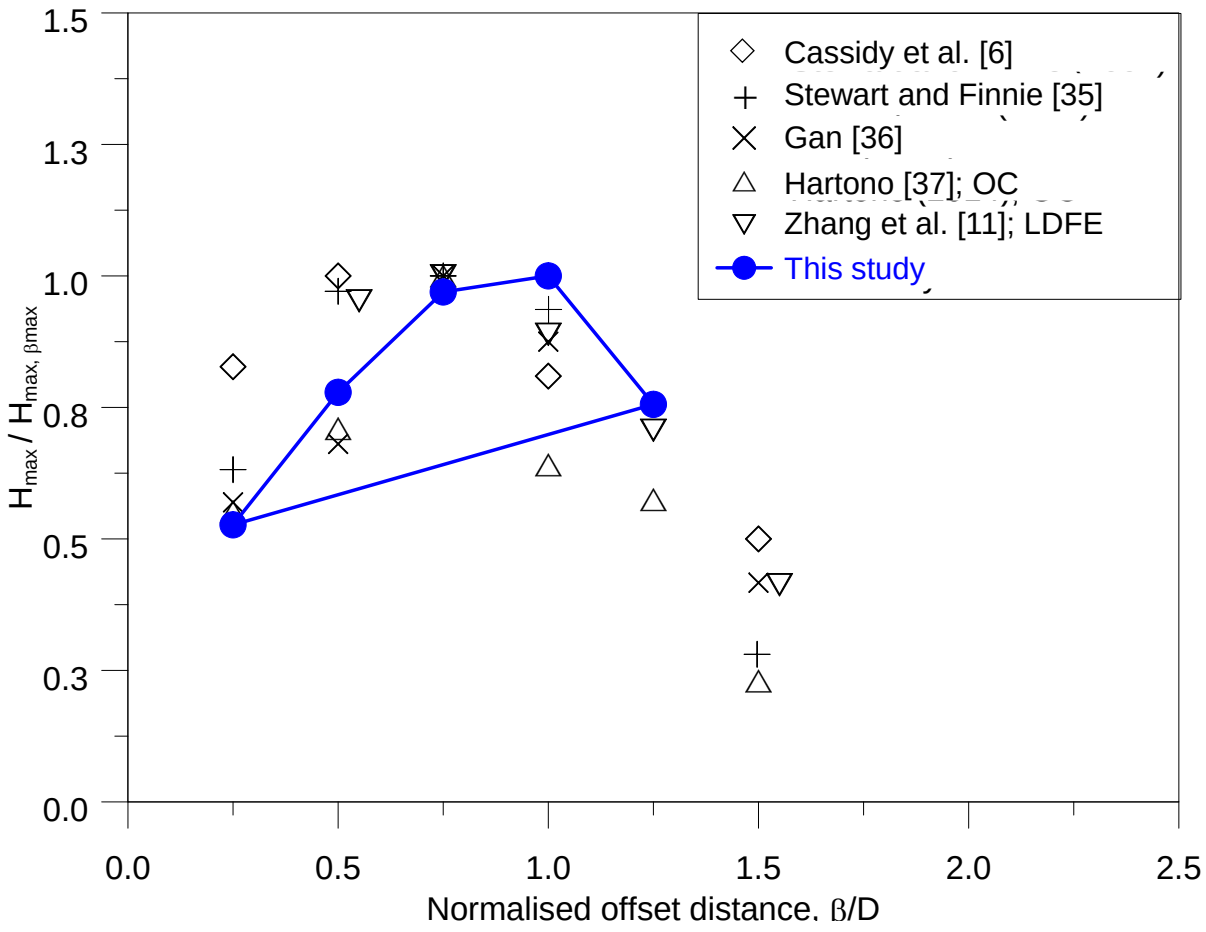

Fig. 15. Comparison of H_{max} with results from previous studies

Submitted Aug. 2019;
Resubmitted Nov. 2019; Re-resubmitted Mar. 2020

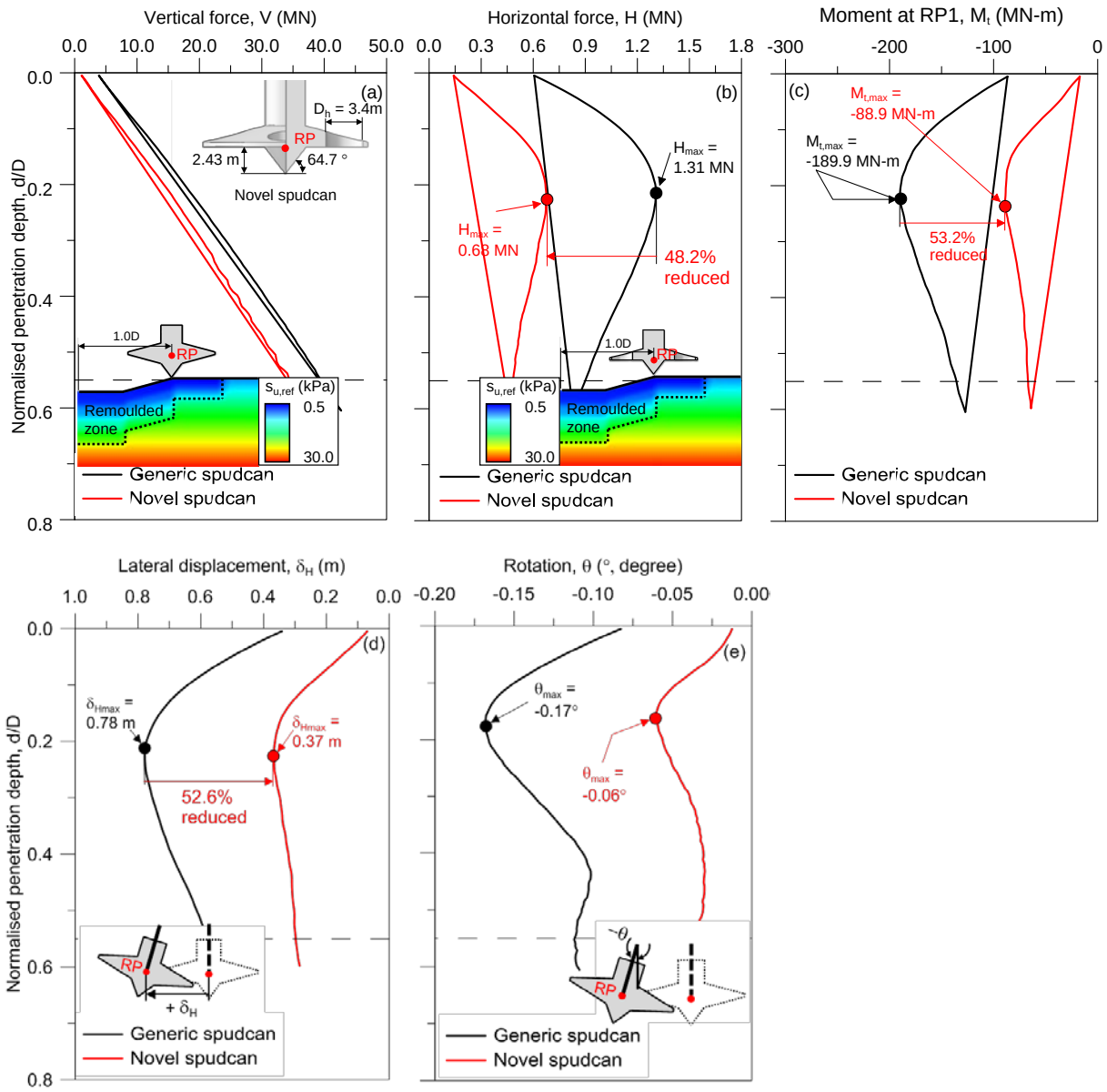

Fig. 16. Responses for generic and novel spudcan: (a) vertical resistance force; (b) horizontal resistance force; (c) moment resistance at RP1; (d) lateral displacement; (e) rotation

Submitted Aug. 2019;
Resubmitted Nov. 2019; Re-resubmitted Mar. 2020

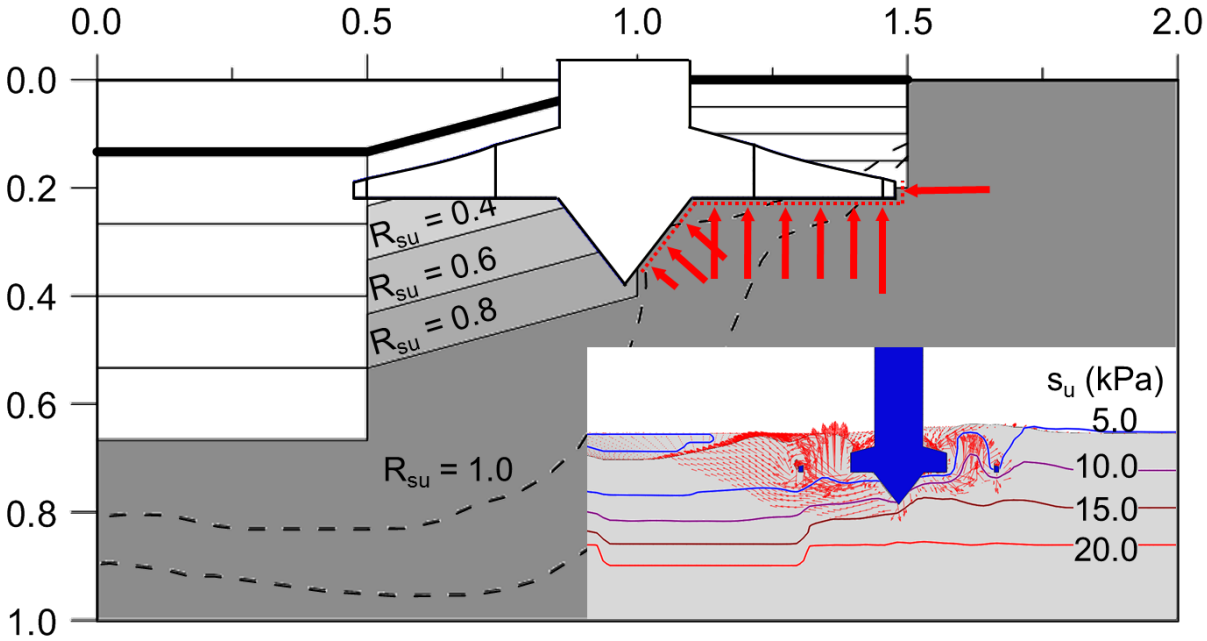

(a) Schematic diagram of imbalance force, failure mechanism and contour line for soil strength: novel spudcan at H_{max} (d_{Hmax}/D = 0.22)

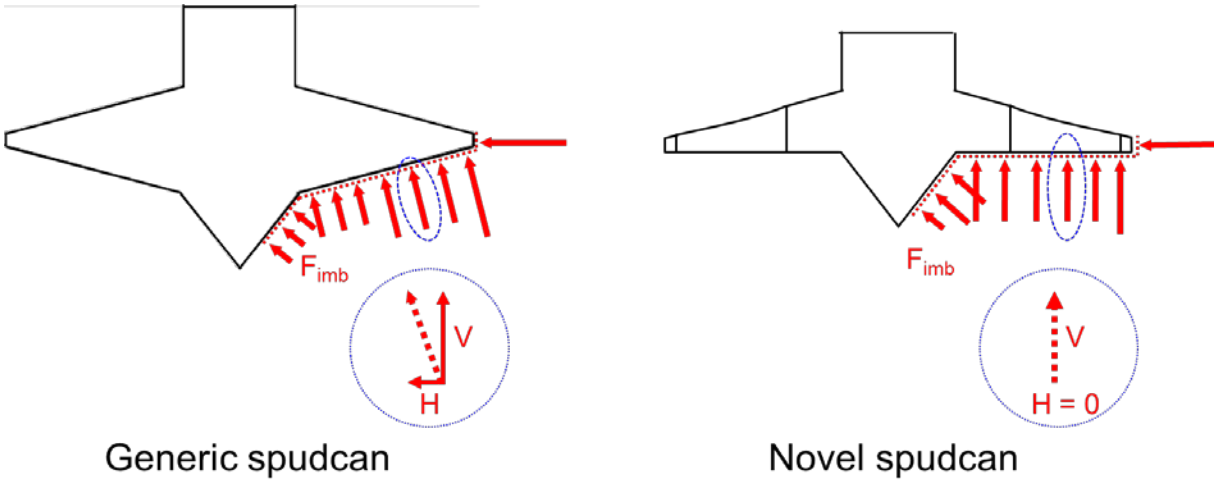

(b) Schematic diagram of imbalance force for generic and novel spudcan

Fig. 17. Schematic diagram of imbalance force

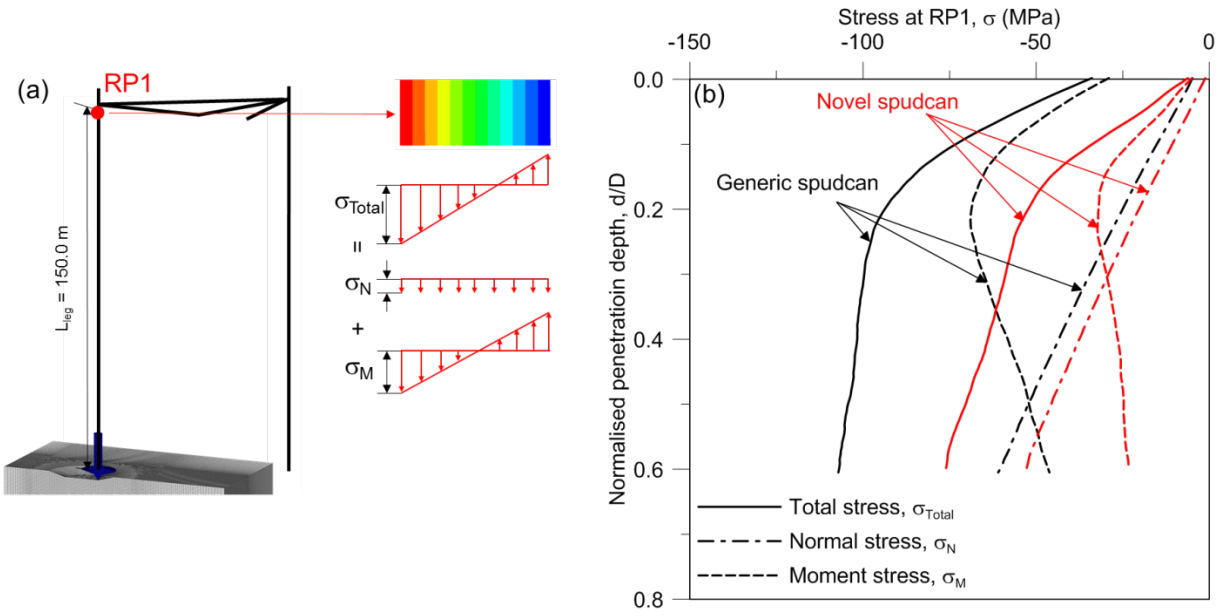

Fig. 18. The effect of novel spudcan on the leg just below hull: (a) structural beam stress (b) reduction of structural beam stress attributed by novel spudcan